The Effect of Dimensional and Material Non-Uniformity on the Development of Triaxial Stresses in Cylinders

by

William Hawkesworth

A thesis submitted to the Faculty and the Board of Trustees of the Colorado School of Mines in partial fulfillment of the requirements for the Master of Science Degree in Metallurgical Engineering.

Signed: Wm. Hawkesworth

William Hawkesworth

Golden, Colorado

Date: November 12, 1968

Approved: J. D. Lubahn

J. D. Lubahn
Thesis Advisor

Paul G. Herold

P. G. Herold, Head
Department of Metallurgical Engineering

Golden, Colorado

Date:

Acknowledgments

The author expresses sincere gratitude to Dr. J. D. Lubahn for his advice and interpretative guidance during this investigation.

The author is indebted to Dr. P. G. Herold and Dr. A. W. Schlechten, Head and former Head, respectively, of the Department of Metallurgical Engineering and to the additional members of his graduate committee: Professors R. B. Bowersox and H. Frost, Jr.

Thanks are due Dr. N. C. Schieltz and Mr. R. Tuffing for their contributions as well as to Mrs. Frances Stewart for her photographic work.

The author also wishes to acknowledge the financial assistance provided by a part-time instructorship, CSM Foundation research grants, and U. S. Air Force contract 29(601) - 6042.

Table of Contents

Table of Contents - cont'd

Abstract

This thesis consists of theoretical and experimental determinations of the plastic triaxiality (restraint) in a cast solder layer bonded between steel end pieces and axially loaded in compression. The work was directed toward a range of practical problems such as short pulses in impact loading and soft welds between harder base metal.

The theoretical triaxiality determination was for the ideal case of an infinitesimally thin solder layer. It was found that the triaxiality increased from 0.345 in the elastic region to 0.76 at 0.002 plastic strain. The experimental values of triaxiality were equal to or higher than the theoretical value for joint thickness-to-diameter ratios in the 0.02 - 0.05 range. For thicker joints the triaxiality was found experimentally to decrease and become quite small at a ratio of unity, as expected from St. Venant's principle. The practical value of the thesis is the experimental curve of triaxiality versus thickness-to-diameter ratio.

As expected, it was found that the plastic behavior depended on strain rate and on the aging time following casting, and these effects were taken into account in the analysis. Unexpected, however, were the results that the modulus of elasticity of the solder depended on the strain rate and that the joints were elastically stiffer than all-solder specimens would indicate. No explanation for either of these effects could be found.

List of Symbols

a = as a subscript denotes axial direction

A = area

C_f = compliance of a test fixture

C_m = compliance of testing machine

$C = C_m + C_f$ (combined fixture and machine compliance)

e = elastic strain

E = modulus of elasticity

E_c = composite modulus

j = as a subscript denotes the solder portion of a joint specimen

l = length (axially)

n = rate sensitivity = $d \log S / d \log \dot{\epsilon}$

P = load

Q = unloaded crosshead speed

r = as a subscript denotes the steel portion of a joint specimen ("rod")

R = triaxiality in the solder portion = S_{tj}/S_a

S = stress

t = time

t = as a subscript denotes the transverse direction

X = axial distance from solder-steel interface

α = a constant

δ = deflection = $\ell \lambda$

List of Symbols - cont'd

Δ = finite change in a variable

ϵ = plastic strain

λ = total strain = $e + \epsilon$

μ = Poisson's ratio

∞ = infinity

zero - as a subscript denotes uniaxial conditions

zero - as a superscript refers to steel-solder interface

dot - over a symbol denotes time derivative

Introduction

This investigation began as part of a general problem concerned with the material behavior of, and energy propagation in, metallic bodies subjected to intense shock wave loading (Houidobre, 1965; Lubahn, et al, 1965; Fiftal, 1967). Such energy pulses may arise from high velocity impact, high explosive attack, or a short pulse of high energy density radiation.

The purpose was to determine the magnitude of stress triaxiality developed in an axially loaded cylinder with a non-uniform diameter (notched), a discontinuity in material properties, or a short stress pulse. In the loading of such structures, the lateral strain of the more easily deformable or more highly stressed section is restrained by its connection to, and its compatability with, an adjacent section that has less tendency to deform. This combination of loading and restraint generates a system of triaxial stress and strain, particularly in the thin, restrained section.

The evaluation of notch stresses in elastic materials has been made for various conditions of geometry and loading (Neuber, 1937; Peterson, 1953). Plastic strain distribution for notched tensile

specimens has been determined (Sachs and Fried, 1949). The state of triaxial stress in a necked tensile specimen has been investigated theoretically by Bridgman (1944) and experimentally by Parker, et al, (1946).

The solution for diametral non-uniformity, which can be found in Appendix 1, is an analytical extension of a previous experimental technique.

The material discontinuity specimens were pairs of hardened, round steel end pieces linked together coaxially with various lengths of solder (butt-soldered joints). These specimens were considered to have a distribution of axial strain that was radially uniform, as with a short pulse in dynamic loading. The thickness of the solder zone may be considered analogous to pulse length. Performance of such specimens in tension may be related to spalling on the rear face of a metallic wall subjected to explosive attack. Work on the butt-soldered joint has been suggested in the literature (Orowan, 1946; Lubahn, 1947).

Specimen Preparation

The determination of both uniaxial and multi-axial behavior in this investigation required the manufacture of a series of high-quality, cast solder tensile specimens and cast, butt-soldered compression specimens.

Tensile Specimens

Button-ended specimens, 5¼-inch-long with a ½-inch-diam by 4-inch-long gage length and 1-inch-diam ends were cast horizontally in a machined steel mold. The mold, which had a riser at each end and a tapered sprue, was preheated to 420° F and filled with solder at 500° F. Commercial grade 50 percent lead, 50 percent tin solder was poured from a cast iron teapot ladle. The center of the poured mold was cooled with a water spray to avoid shrinkage voids and to produce a specimen solidification cooling rate similar to the cast joint (125° F/min). This was done to make the as-cast hardnesses of the uniaxial and joint specimens equal (same micro-structure). The gage lengths of the specimens were turned and polished on a lathe to provide a uniform diameter, a flat seat for the testing machine fixtures, and a suitable surface for microhardness testing. All specimens tested were free from discernable shrinkage, gas holes, and discontinuities.

Butt-Soldered Joints

The joint specimens consisted of two pieces of ground, hardened steel bar stock, 1-inch-diam. and 1¼-inch-long, linked together as concentrically as possible with a uniform length of commercial grade 50 percent lead, 50 percent tin solder. A slightly reduced section, spanning the joint, was ground on the specimen to measure joint thickness, solder hardness and deformation.

Two-specimen bars 2 5/8-inch-long were machined from a 1-inch-nominal diameter hardenable steel rod as single pieces with each end faced flat, chamfered and center-drilled. Drill rod could be made hard enough for the long solder joints. Ketos tool steel was used for the shorter joints. The center holes fitted the floating balls on the ends of the assembly fixture screws. The chamfered ends permitted assembly of the bars without damage to the mold seal rings. After hardening and tempering at 600° F, the bars were centerless ground to $1.000\ ^{+0.000}_{-0.002}$ inch. The ground pieces were match-marked for assembly coordination and were cut into two 1¼-inch-long pieces using the abrasive cutting machine with an alundum wheel and a copious water spray. The hardness of the cut faces of the Ketos and drill rod measured Rockwell 'C' 51 and 43 min, respectively. The abrasive-cut surfaces were smooth enough and square enough to be suitable for the solder joint.

Prior to joining, the bar ends adjacent to the joint were tinned by dipping the preheated (450° F) bars into flux-covered solder at 450° F. The bar was examined to ascertain that there was complete wetting by the solder. The tinned end was held in flux-covered solder

for 90 min. at 450° F to form a surface layer of Sn-Fe compound. The composition and kinetics of compound formation were given by U.S. Steel (1957). This "soaking" treatment was found necessary to achieve optimum joint bonding. The liquid and loose solid material was removed from the "soaked" bars by shaking and wiping, and the bars were retinned in fresh, flux-covered solder to avoid build-up of iron concentration in the solder-joint. Solder on the sides of the bars was removed by wiping them when they were hot and by rubbing them with abrasive paper after they had cooled.

The flux used for tinning and joint assembly was an eutectic mixture of 71 percent $ZnCl_2$ and 29 percent NH_4Cl, with a melting point of 354° F (Hiers and Schumacher, 1948). The composition was adjusted by making the freezing point a minimum. A minimum freezing point below that of solder was desirable to avoid trapping of solid flux. This flux produced rapid and complete tinning of the bars which had an oxide film from the 450° F preheat. When flux was used during preheating of the bar-mold assembly, a vigorous reaction occurred at first, and this produced a poorly-bonded joint which was filled with blow holes. For this reason, the flux was applied for about 2 min before the joint was poured.

After tinning, the bars were assembled in the mold and support fixture (see Fig. 1). Concentricity was accomplished by holding the bars in the vee block with spring-loaded, asbestos-cushioned levers. Flat-ended adjusting screws, with captive floating balls which fitted the center-drilled bars, provided axial adjustment of the bars without affecting their vee block alignment. The screws, with jam nuts set

to control joint thickness, were retracted for assembly and adjusted to provide about 1/8-inch space between the bars for pouring the joint.

The two-piece mold for casting the joint was machined from graphite (see Fig. 2). It was parted normal to the bar axis and had a tapered sprue, gating, a riser and an overflow. In each mold-half, the bar was sealed by a 0.048-inch-thick Teflon back-up ring (inboard) and a 3/32-inch-diam Viton "O" ring (outboard), which were retained in an annular groove. The mold halves were sealed with a piece of 1/8-inch-diam silicone rubber rod resting in a groove in one mold half. The halves were matched with two locating pins and screwed together. Silicone grease, Teflon spray, and molybdenum disulfide were used as mold release agents.

The following steps were used to make the joint (see Fig. 3):

1. Two tinned bars were assembled in the mold and fixture with a 1/8-inch-minimum pouring gap and the screws adjusted for desired joint thickness.

2. The assembly, with asbestos blankets on the mold, was heated to 430° F in a furnace.

3. The heated assembly was removed from the furnace and filled with fresh flux at 450° F.

4. After 2 minutes, the mold was filled with solder at 600° F through the sprue, flushing flux and excess solder up the riser and out the overflow into a container.

5. The top mold blanket was applied, and the screws were adjusted for joint thickness.

6. The vee blocks and fixture base were cooled with a water spray. Because of the fixture mass, forced cooling and mold insulation were essential in producing shrinkage in the riser rather than in the joint. Thermocouple tests of several joints showed a cooling rate of about 125° F/min between the liquidus (421° F) and solidus (361° F) for the solder.

7. The cast joint specimen was removed from fixture and mold. (See Fig. 4 for specimen with sprue and riser.)

In order to avoid iron contamination of the solder joint, the flux and solder for the joints were handled in porcelain ware and a graphite teapot ladle. The solder used for soaking the bars was kept separate. Thermocouple contamination was avoided by the use of a Vycor protection tube.

The cast joint specimens were prepared for testing by machining off the excess solder and grinding (specimen held in centers) a 3/4-inch-long section at mid-length to make a gage length (see Fig. 4). Spiral polishing, with metallographic paper to a 4/0 finish, permitted the measurement of joint thickness and Knoop hardness. The specimens were equipped with two pairs of soldered seats, spaced ½-inch apart axially, and diametrically opposite, to support the Huggenberger strain gages.

Trial joints were made and fractured by bending to determine the quality of casting and bonding. Optimum bonding was determined by a high relative moment to produce fracture and by the gray, matte appearance of the fractured faces. This appearance was due to a high density of solder particles adhering to the steel face. The fact that the

particles were solder, and not steel, was ascertained by scratching the steel surface with a hardened needle-like pick under a high-power binocular microscope. The efficacy of spray-cooling and "solder-soaking" was shown by achievement of optimum quality.

Experimental Procedure and Data

The phases of the program were:

1. To determine the stress state of butt-soldered joints of various lengths by experimental means.

2. To analyze the infinitely thin joint for the elastic and plastic conditions.

For this investigation, it was assumed that both axial and transverse stresses and strains would be uniform throughout the joint.* The numerically largest, principal, plastic strain was taken as the measure of strain hardening. The shear stress law, the constant volume condition, the compatability condition, Hooke's law for multi-axial stress, and equilibrium of force principles were applied.

In order to use these laws and principles, values of flow stress, Young's modulus and Poisson's ratio were required for the solder in the joint as affected by the test conditions of age, strain, and strain rate. Only the hardness of the solder at the joint surface could be measured directly for comparison with other specimens and tests. Tensile tests of solder bars, which had a solidification history as nearly

* According to St. Venant's principle, this should be true except up to depths, below the surface, that are comparable with the joint length.

identical to the joints as possible, were also made to evaluate the strength of the solder in the joint.

Tensile Tests

The Baldwin machine, equipped with button-head fixtures and the 2-inch, SR-4 extensometer, was used to test the cast solder specimens. The calibrated speed control (see Appendix 2) was set to produce the desired nominal strain rate. Actual strain rates were determined from the plotted data by use of compliance methods.

Rate-Change Tests

In a preliminary investigation of strain rate and aging, a button-head, all-solder specimen was subjected to several strainings, each followed by a period of aging at room temperature. Each straining was conducted at two or more rates, the rate being changed abruptly by means of the speed control.

The data are shown in Table 1. It is evident from the stress levels following the aging periods that softening (recovery) had occurred during the resting period, although the phenomenon of recovery was not studied specifically during this investigation.

As a result of a sudden speed change the load-strain curve rose in a transient, and then took the same steady-state slope as the lower rate curve. The upper steady-state curve was extrapolated back to the strain at which the rate was suddenly changed, and the corresponding stress is shown as "strength" in the table. The load for the slower rate was

also determined at the same strain. The stress ratio was obtained from the sudden shift in steady-state load, and the logarithm of this ratio was plotted against the logarithm of the rate ratio in Fig. 5. The head speed ratio could be used as the strain rate ratio in this case because the load changes were small. In test C-4-4, the stress data for the speed change from 5 to 28 mil/min were corrected to 3.4 percent plastic strain.

Relation Between Hardness and Yield Strength

As discussed previously, the cooling rates for both tensile and joint specimens was adjusted to 125° F/min. to insure equal properties of the solder in the two types of specimens. To make sure that equal properties really were being obtained by this procedure, Knoop microhardness impressions were made in the polished cylindrical surfaces of both types of specimens. Since impression size was limited by the 0.020-inch-long joint, the impressions were made with 100 gm load. The long axis of the indenter was parallel to the length of the specimen. Comparative tests on flat and ½-inch-diameter cylindrical surfaces of the same piece of solder showed that, for these conditions, curvature had no effect on the hardness determination.

The hardness measurements on the tensile type specimens were made on specimens which had aged various times since having been cast, and the yield strengths of these specimens also were determined (Table 2). From this data, the hardness-yield strength relationship (fig. 6) and the aging effects (Fig. 7) could be determined.

Effect of Strain Rate on Young's Modulus

In tensile tests of cast solder, the slope of the initial, linear portion of the stress-strain curve (and Young's modulus) increased with an increase in strain rate. Perceptable plastic deformation occurred at about 1000 psi (200 lb) at a strain rate of 1.2×10^{-5} sec^{-1} and 1400 psi (250 lb) at a strain rate of 20×10^{-5} sec^{-1}. The SR-4 extensometer was capable of resolving a strain of 20×10^{-6}. This soft material required the use of the 100 lb and 500 lb load scales to improve the accuracy of the measured modulus by developing longer linear curves.

A series of hysteresis tests was also made on one specimen using these scales and a variety of strain rates from 0.83×10^{-5} to 19.7×10^{-5} sec^{-1}. The linear portions of the load-strain curves were from 40 to 100 percent of full scale. These results, together with modulus values from conventional yield strength tests, are plotted on Fig. 8. In one test, the strain rate was measured directly from chart time marks. The rates for the other tests were computed from machine-rate and compliance. The graph shows that good agreement was obtained by the two methods of testing and by the two methods of determining strain rate.

Poisson's Ratio

A cast solder tensile specimen $\frac{1}{2}$-inch by 2-inch by 7-inch was tested in tension to determine Poisson's ratio. In each of two continuous tests, one for longitudinal strain and one for transverse strain

(2-inch dimension), the two Huggenberger gages and the load dial were read in succession at 15 sec intervals. The head speed was set for 2.52 mil/min. Longitudinal strain rate was measured at 3.65×10^{-8} sec^{-1}. Young's modulus and Poisson's ratio were 2.49×10^{6} psi and 0.277, respectively. This combination of modulus and strain rate is not consistent with Fig. 8. The higher modulus value may have been due to the transverse restraint of the grips, which had a 1-inch "bite" on the specimen, to produce a gage length only $2\frac{1}{2}$ times the width.

Compression Tests on Steel Pieces

Compression tests were made on the uncut $2\frac{1}{2}$-inch-long, 1-inch-diam, hardened, tempered and ground specimens of drill rod and Ketos steel, using a maximum stress of 63,700 psi. The values of Young's modulus were 30,400,000 psi, and 29,600,000 psi, respectively. Yielding did not occur, thus showing sufficient hardness for the purpose. In the analysis, the modulus of the steel will be taken as the average of the above values: 30,000,000 psi.

Testing of Butt-Soldered Joints

Except for a few preliminary tensile specimens, all of the joints were tested in compression. The triaxiality effects in both type specimens would be expected to be similar, except that the ductility of the tension specimen would be lower due to the tensile stress state. Compression specimens were more convenient to prepare and test.

The Tukon machine was used to measure the joint length of each ground and polished specimen at eight places. These data were averaged for each joint.

Longitudinal deformation of the specimen during compressive loading was measured by a pair of Huggenberger gages ($\frac{1}{2}$-inch-gage length; sensitivity, 2000 x) attached to the specimen across the joint. The Baldwin machine was equipped with a levelling compression fixture, which consisted of one fixed head and one spherically-seated head. Prior to testing, the specimen was centered and the fixture was levelled to the flat-ground ends of the specimen. Further fixture alignment for uniform loading was made by applying a 10-lb compressive load and tapping the spherical fixture. Fig. 9 shows the experimental arrangement. The data are shown in Table 3 and Figs. 10-14.

Analysis

The classical principles of material behavior were used to examine the soldered joint. This was done to validate the implied assumptions in the experimental determination, to compare the theoretical and experimental results, and to appraise the limits of these approaches.

Analysis of Elastic Strain Rate for Joint Tests

In both the elastic and plastic regions, the strain rate was determined from the dial setting on the Thymatrol Drive, which determines the motor speed, and the compliance of the testing machine and the test fixtures. With no load on the machine, all of the angular motion of the motor shaft manifests itself as crosshead motion. When a specimen is being loaded, part of the angular motion of the shaft is used in deflecting the gears and other machine parts and some shows up as crosshead motion. The crosshead motion is used up partly in straining the specimen and partly in causing deflection of the fixture. Thus, the amount of shaft motion, expressed in terms of the unloaded crosshead speed, can be divided into machine deflection,

fixture deflection, and strain in the specimen. The strain in the specimen can be divided into that in the steel and that in the solder, and the strain in the solder might have both an elastic part and a plastic part. These physical facts can be expressed mathematically by the equation:

$$Qt = Pc_m + Pc_f + l_r e_r + l_j e_j + l_j \epsilon_j \qquad (1)$$

where:

Q = unloaded crosshead speed

t = time

P = load

c_m = compliance of the testing machine

c_f = compliance of the test fixture

l_r = combined length of the steel end pieces

l_j = length of solder joint

e_r = axial elastic strain in the steel

e_j = axial elastic strain in the solder

ϵ_j = axial plastic strain in the solder

For the elastic case we are considering here, $\epsilon_j = 0$. Also P may be factored out of the first two terms of the right-hand side, leaving the sum of machine and fixture compliance, and this sum may be represented by the single symbol C.

$$Qt = Pc + l_r e_r + l_j e_j \qquad (2)$$

Differentiating with respect to time

$$Q = c\frac{dP}{dt} + l_r \frac{de_r}{dt} + l_j \frac{de_j}{dt} \qquad (3)$$

If both steel and solder are in uniaxial compression, *

$$e_j = \frac{S}{E_j} = \frac{P}{AE_j} \tag{4}$$

$$e_r = \frac{S}{E_r} = \frac{P}{AE_r} \tag{5}$$

from Hooke's law. A is cross sectional area and E_j and E_r are modulus for solder and steel respectively, and S is stress. Differentiating (4) and (5), substituting into (3), and solving for de_j/dt,

$$Q = cAE_j \frac{de_j}{dt} + \frac{l_r}{AE_r}\frac{dP}{dt} + l_j \frac{de_j}{dt}$$

$$Q = cAE_j \frac{de_j}{dt} + \frac{l_r}{AE_r}\left(AE_j \frac{de_j}{dt}\right) + l_j \frac{de_j}{dt}$$

$$\frac{de_j}{dt} = \frac{Q}{Ae_jc + l_r(E_j/E_r) + l_j} \tag{6}$$

Equation (6) has to be solved graphically because of the fact that E_j is a function of strain rate. This is done by starting with an arbitrary initial set of values of strain rate, finding the corresponding moduli from Fig. 8, substituting into equation (6) to find a final set of values of strain rate, plotting both initial and final rates against E_j, and reading off the intersection point. The procedure is illustrated below for test K-12, for which $Q = 8.33 \times 10^{-5}$ sec^{-1}, $l_j = 0.020$ in., $l_r = 2.36$ in., $A = 0.759$ in^2, $E_r + 30 \times 10^6$ psi $C_m = 1.03 \times 10^{-6}$ in./lb, and $C_f = 0.016 \times 10^{-6}$ in./lb.

---

* Appendix 3 shows that this approximation is close enough, in the case of the steel, for any purposes. Appendix 4 shows that, for the present purposes, the approximation of uniaxiality in the solder is also good enough.

$\frac{de_j}{dt}$ (sec^{-1})	E_j (psi)	AE_jC	$\ell_n\left(\frac{E_j}{E_n}\right)$	Denominator	$\frac{de_j}{dt}$ (sec^{-1})
1×10^{-5}	1.85×10^6	1.47	0.15	1.64	5.08×10^{-5}
2×10^{-5}	2.65×10^6	2.11	0.21	2.34	3.55×10^{-5}
5×10^{-5}	3.44×10^6	2.74	0.27	3.03	2.75×10^{-5}
10×10^{-5}	3.87×10^6	3.08	0.30	3.40	2.45×10^{-5}
20×10^{-5}	4.21×10^6	3.35	0.33	3.70	2.25×10^{-5}

The graphs are shown in Fig. 15. From the intersection point, we find that the strain rate was 3.1×10^{-5} sec^{-1} and the modulus of elasticity of the solder was 3.05×10^6 psi.

By applying the same method to the other tests, the rates and modulus values were found as shown in Table 4.

Elastic Stiffness for the Case of Full Restraint

For a sufficiently thin joint, the solder will be completely restrained from moving radially by any more than the steel moves radially, that is, the transverse strains in the steel and solder will be equal. This fact is expressed mathematically by:

$$e_{tr} = e_{tj} + \epsilon_{tj} \qquad (7)$$

where subscript t denotes the transverse direction, subscripts r and j denote the steel and solder respectively, and e and ϵ denote elastic and plastic components of the strain respectively.

For this case of full restraint the steepness of the elastic load-deflection curve (elastic stiffness) can be calculated. This will be done, and the result will be compared with the experimental result for the thinnest joint.

The thinnest joint is 0.020 inches thick (test K-12). From the faired elastic line in Fig. 10 we find that the average compressive strain on a ½-inch gage length is 0.00079 at a compressive load of 15,500 pounds. The cross-sectional area is 0.759 in^2. From these values we can find the elastic stiffness as

$$E_c = \frac{S}{e_{av}} = \frac{P}{A e_{av}} = \frac{15,500}{(0.759)(0.00079)} = 25.9 \times 10^6 \text{ psi}$$

This value will be referred to as the "composite modulus" because it involves two materials. It will depend on the relative lengths of the two materials contained within the gage length, as well as the moduli of the two materials.

The theoretical value of composite modulus can be determined with the aid of equation (7). For the case at hand, $\epsilon_{tj} = 0$ and

$$e_{tr} = e_{tj} \tag{8}$$

These elastic strains can be determined from Hooke's law. We can neglect* the transverse ** stress in the steel, for purposes of applying Hooke's law, but the transverse stress in the solder cannot be neglected.

$$e_{tr} = \frac{S_{tr} - \mu_r (S_{ar} + S_{tr})}{E_r} = -\frac{\mu S_a}{E_r} \tag{9}$$

$$e_{tj} = \frac{S_{tj} - \mu_j (S_{aj} + S_{tj})}{E_j} = \frac{S_{tj}(1-\mu) - \mu S_a}{E_j} \tag{10}$$

---

* See Appendix 3.

**The two transverse stresses, radial and tangential, are taken as equal here.

Subscripts r and j are unnecessary on μ because the values of Poisson's ratio happen to be the same for steel and solder. Also, subscripts r and j are unnecessary on S_a because the series arrangement of the two materials requires the axial loads to be the same, by virtue of force equilibrium, and since the cross-sectional areas are the same the axial stresses will be equal.

Equations (8), (9) and (10) permit us to find the magnitude of the transverse stress in the solder. Substituting (9) and (10) into (8) and solving for S_{tr}, we obtain

$$S_{tj} = \frac{\mu S_a}{1-\mu}\left(1 - \frac{E_j}{E_r}\right) \qquad (11)$$

This value of transverse stress* can now be used to find the axial strain in the solder, which together with the axial strain in the steel, govern the composite modulus. Applying Hooke's law again, this time to the axial strains, we obtain

$$e_{ar} = \frac{S_a}{E_r} \qquad (12)$$

$$e_{aj} = \frac{S_a - \mu(S_{tj} + S_{tj})}{E_j} = \frac{S_a - 2\mu S_{tj}}{E_j} \qquad (13)$$

The composite modulus is

$$E_c = \frac{S_a}{e_{av}} = \frac{S_a}{(\delta/l)} = \frac{S_a l}{\delta} = \frac{S_a l}{\delta_r + \delta_j} = \frac{S_a l}{l_r e_r + l_j e_j} \qquad (14)$$

where l is the whole gage length, l_r and l_j are the portions of the gage length composed of steel and solder respectively, δ is the deflection of the whole gage length, and δ_r and δ_j are the

* Note that the elastic triaxiality, S_{tj}/S_a, is

$$\frac{S_{tj}}{S_a} = \frac{\mu}{1-\mu}\left(1 - \frac{E_j}{E_r}\right)$$

which is 0.345 for μ = 0.277 and E_j/E_r = 0.1

contributions to that total deflection that are contributed by the steel and solder respectively.

Substituting (11) into (13), and then substituting this result and (12) into (14), we obtain

$$E_c = \frac{l}{\frac{l_r}{E_r} + \frac{l_j}{E_j}\left[1 - \frac{2\mu^2}{1-\mu}\left(1 - \frac{E_j}{E_r}\right)\right]} \qquad (15)$$

For test K-12, l_j = 0.020 in. and l_r = 0.480 in., making up a total gage length (l) of 0.500 in. As discussed previously, Poisson's ratio for solder was determined as 0.277, and since Poisson's ratio for steel is generally taken as 0.28, both materials were assigned the same value of Poisson's ratio in this analysis, namely 0.277. As discussed previously, E_r was measured as 30.0×10^6 psi, and from Table 4 E_j for this test is 3.05×10^6 psi. For these values, (15) yields a value of composite modulus of 23.5×10^6 psi.

Note that the measured composite modulus (25.9×10^6 psi) is somewhat higher than the calculated composite modulus (23.5×10^6 psi). This means that the joint specimen is elastically more stiff than one would expect on the basis of the moduli of the two materials separately. The difference is not startling; in fact, the statistical significance of the difference could be questioned when one considers the small amount of data. We shall see later, however, that this difference exists for all the joint tests, not just K-12.

Equation (15) also permits us to find what value of E_j would be necessary to give the observed composite modulus of 25.9×10^6 psi. We expect a larger value of E_j than 3.05×10^6 psi; this larger value

is the mathematical equivalent of the physical statement that "the joint specimen is elastically more stiff than one would expect on the basis of the moduli of the two materials separately". Substituting 25.9×10^6 for E_c and, except for E_j, the same values as before, and solving for E_j, we find $E_j = 4.94 \times 10^6$ psi. In the plastic analysis this value will be used, so that the elastic lines will coincide when comparing measured and calculated behavior in the plastic range.

Uniaxial Plastic Properties

The stress necessary to cause continuing plastic deformation of the solder in uniaxial tension will be a function of plastic strain, plastic strain rate, and aging time. This three-variable function is the basic information needed for plastic analysis of the joint tests later. The function will be expressed as a curve of stress versus plastic strain for one particular combination of strain rate and aging time, together with two additional curves that provide correction factors for strain rate and aging time. The correction factors for strain rate and aging time are obtained from Figs. 5 and 7. The stress-strain curve for a given strain rate and aging time will now be determined from the data of test C-12.

Test C-12 was a tensile test of a button-head specimen tested ten (10) days after casting. The four-inch length between the button heads was uniform in cross sectional area at 0.182 in^2. The unloaded cross-head speed was 0.208×10^{-3} sec^{-1}. The tensile testing fixtures

that were used had a compliance of 5.44×10^{-6} in./lb., and in the range of load for this test the machine compliance was 0.77×10^{-6} in./lb. From the load-deflection curve, the elastic and plastic strains were determined at various points during the test, as follows:

Load (lb.)	Stress (psi)	Plastic Strain (10^{-3})	Elastic Strain (10^{-3})	Total Strain (10^{-3})
200	868	0	0.275	0.275
525	2880	0.50	0.92	1.42
640	3520	1.00	1.12	2.12
705	3870	1.75	1.23	2.98
720	3960	2.00	1.26	3.26

As before, the strain rates are determined from the unloaded crosshead speed and the compliance. For this case, where the specimen was all solder, equation (1) reduces to

$$Qt = Pc + \ell\lambda = SAc + \ell\lambda \tag{16}$$

where λ is total strain ($e + \epsilon$). Differentiating and rearranging,

$$Q = cA\frac{dS}{dt} + \ell\frac{d\lambda}{dt} = cA\frac{dS}{d\lambda}\frac{d\lambda}{dt} + \ell\frac{d\lambda}{dt} \tag{17}$$

Solving for $d\lambda/dt$

$$\frac{d\lambda}{dt} = \frac{Q}{cA\frac{ds}{d\lambda} + \ell} \tag{18}$$

For the case at hand, Q = 0.000208, C is $5.44 \times 10^{-6} + 0.77 \times 10^{-6} = 6.21 \times 10^{-6}$, A = 0.182, l = 4, and the values of $ds/d\lambda$ can be obtained from a graph (Fig. 16.) of stress versus total strain plotted from the table above. Taking slopes and substituting into (18), we

obtain:

S (psi)	$dS/d\lambda$ (10^6 psi)	$CA(dS/d\lambda)$ (in.)	$(CA\frac{dS}{d\lambda}+\ell)$ (in.)	$\frac{d\lambda}{dt}$ (10^{-5} sec^{-1})
0	3.14	3.55	7.55	2.75
1000	3.14	3.55	7.55	2.75
1500	2.04	2.30	6.30	3.30
2000	1.75	1.98	5.98	3.48
2500	1.33	1.50	5.50	3.78
3000	1.08	1.22	5.22	3.98
3250	0.90	1.02	5.02	4.14
3500	0.68	0.77	4.77	4.36
3750	0.41	0.46	4.46	4.66
4000	0.18	0.20	4.20	4.95

These total strain rates can be regarded as being composed of an elastic part (de/dt) and a plastic part ($d\epsilon/dt$). We are interested in the plastic part here. Since

$$\lambda = e + \epsilon \tag{19}$$

$$\frac{d\lambda}{dt} = \frac{de}{dt} + \frac{d\epsilon}{dt} \tag{20}$$

$$\frac{d\epsilon}{dt} = \frac{d\lambda}{dt} - \frac{de}{dt} = \frac{d\lambda}{dt} - \frac{1}{E}\frac{dS}{dt} = \frac{d\lambda}{dt} - \frac{1}{E}\frac{dS}{d\lambda}\frac{d\lambda}{dt} = \frac{d\lambda}{dt}\left(1 - \frac{1}{E}\frac{dS}{d\lambda}\right) \tag{21}$$

thus giving the plastic strain rate. These rates, together with the corresponding values of stress and plastic strain, are given below.

S (psi)	ϵ (10^{-3})	$d\epsilon/dt$ (10^{-5} sec^{-1})
0	0	0
1000	0	0
1500	0.05	1.16
2000	0.15	1.54
2500	0.32	2.18
3000	0.58	2.62
3250	0.75	2.96
3500	1.00	3.42
3750	1.45	4.05
4000	2.25	4.66

Now we have stress versus plastic strain, but for a variable rate rather than a constant rate as was desired. A curve for constant rate can be constructed by taking advantage of the fact that the slope of the graph in Fig. 5 is 0.115. This slope is called the "strain rate exponent". By definition, it is

$$n = \frac{d \log S}{d \log \dot{\epsilon}} = 0.115 \qquad (22)$$

where $\dot{\epsilon}$ denotes the time derivative. If the graph is linear, as is very nearly so in Fig 5, (22) may be written as

$$n = \frac{\Delta \log S}{\Delta \log \dot{\epsilon}} = \frac{\log S_2 - \log S_1}{\log \dot{\epsilon}_2 - \log \dot{\epsilon}_1} = \frac{\log (S_2/S_1)}{\log (\dot{\epsilon}_2/\dot{\epsilon}_1)} \qquad (23)$$

Now the stress strain curve given by the table above can be corrected to a constant rate of 4.66×10^{-5} sec^{-1} by thinking of subscript 1 in equation (23) as applying to the last row in the table and letting subscript 2 apply successively to each of the other rows as follows:

S (psi)	ϵ (10^{-3})	$\dot{\epsilon}$ (10^{-5} sec.$^{-1}$)	$\frac{\dot{\epsilon}_2}{\dot{\epsilon}_1}$	$\log \frac{\dot{\epsilon}_2}{\dot{\epsilon}_1}$	$\log \frac{S_2}{S_1} = n \log \frac{\dot{\epsilon}_2}{\dot{\epsilon}_1}$	$\frac{S_2}{S_1}$	S_2 (psi)	$\log S_2$	$\log \epsilon$
0	0	0							
1000	0	0							
1500	0.05	1.16	4.01	0.603	0.0840	1.213	1870	3.260	-4.30
2000	0.15	1.54	3.02	0.480	0.0552	1.136	2270	3.356	-3.82
2500	0.32	2.18	2.14	0.330	0.0379	1.090	2730	3.436	-3.50
3000	0.58	2.62	1.78	0.250	0.0287	1.068	3200	3.505	-3.24
3250	0.75	2.96	1.57	0.196	0.0225	1.053	3420	3.534	-3.12
3500	1.00	3.42	1.36	0.134	0.0154	1.037	3630	3.560	-3.00
3750	1.45	4.05	1.15	0.060	0.0069	1.016	3810	3.581	-2.84
4000	2.25	4.66	1.00	0.000	0.0000	1.000	4000	3.602	-2.65

The results are shown in Fig. 17. The stress-plastic strain curve has been plotted on log-log paper for accuracy of reading values,

particularly at small plastic strains. This figure, together with Figs. 5 and 7, give the uniaxial plastic behavior of the solder.

Plastic Analysis of Joint Test - Full Restraint

As discussed earlier, equation (7), strain compatibility between the steel and solder, requires that

$$\epsilon_{tj} + e_{tj} = e_{tr}$$

and equilibrium of force in the axial direction requires that

$$S_{ar} = S_{aj} = S_a \tag{24}$$

Equations (9) and (10) give the required elastic strains as

$$E_j e_{tj} = S_{tj} - \mu(S_a + S_{tj}) = S_{tj}(1-\mu) - \mu S_a$$

$$E_r e_{tr} = 0 - \mu(S_a + 0) = -\mu S_a$$

Appendix 3 shows that the transverse stress in the steel can be neglected, as has been done in the equation (9). Substituting (9) and (10) into (7),

$$\frac{S_{tj}(1-\mu) - \mu S_a}{E_j} + \epsilon_{tj} = \frac{-\mu S_a}{E_r} \tag{25}$$

Applying the shear stress law and associated strain hardening criterion to the joint,

$$S_o = S_{tj} - S_a \tag{26}$$

$$\epsilon_{aj} = -\epsilon_o = -2\epsilon_{tj} \tag{27}$$

where subscript zero denotes uniaxial conditions. Substituting (26) and (27) into (25),

$$\frac{(S_o + S_a)(1-\mu) - \mu S_a}{E_j} + \frac{\epsilon_o}{2} = \frac{-\mu S_a}{E_r} \tag{28}$$

Solving for S_a,

$$S_a = \frac{S_o(1-\mu) + 0.5\epsilon_o E_j}{2\mu - 1 - \mu(E_j/E_r)} \qquad (29)$$

Now the load-deflection curve for a joint test can be calculated, using equation (29), as follows. We let ϵ_o take on a set of arbitrary values and find the corresponding values of S_o from an appropriate $S_o - \epsilon_o$ curve, with proper aging time and any reasonable, constant, plastic strain rate. These values, together with the appropriate elastic properties, are substituted into equation (29) to obtain S_a. As soon as we know S_a, all other quantities can be calculated, including plastic strain rate. If this rate is the same as the initially assumed rate, we have the correct solution; if not, the first calculation may be considered as a first approximation to the solution, the resulting rate taken as the assumed rate for a second approximation, and so on until convergence of the iteration procedure.

The method will be illustrated by applying it to test K-12. For this test, $E_j = 4.94 \times 10^6$ psi, as discussed previously, $\mu = 0.277$ $Q = 8.33 \times 10^{-5}$ sec $^{-1}$, $l_j = 0.02$ in., $l_r = 2.36$ in., $A = 0.759$ in^2, $E_r = 30 \times 10^6$ psi, $C = 1.05 \times 10^{-6}$ in/lb., and the aging time is zero. Since Fig. 17 already gives S_o versus ϵ_o for a plastic strain rate of 4.66×10^{-5} sec $^{-1}$, we will take this rate as the initial rate, for the first approximation. Since the graph in Fig. 17 is for test C-12, with ten days aging, and K-12 is for no aging, the curve of Fig. 17 first has to be corrected for the difference in aging times. This is

done with the aid of Fig. 7. Fig. 7 shows that the solder of test K-12 will be stronger than the solder of test C-12 in the ratio 4500/3950 = 1.14. Since $\log_{10} 1.14 = 0.057$, the curve for no aging and a rate of 4.66×10^{-5} sec $^{-1}$ will be above the curve for test C-12 by 0.057.

The calculations of S_a from equation (29) and the associated times, for an arbitrary set of values of ϵ_o, are shown below.

$\epsilon_o = -\epsilon_{aj}$ (10^{-3})	$\log_{10}\epsilon_o$	$\log_{10} S_o$ for C-12	$\log S_o$ (add 0.057)	S_o (psi)	S_a (psi)
0.050	-4.3	3.265	3.322	2100	-3350
0.063	-4.2	3.279	3.336	2170	-3510
0.080	-4.1	3.298	3.355	2265	-3740
0.100	-4.0	3.314	3.373	2360	-3970
0.126	-3.9	3.336	3.395	2485	-4290
0.159	-3.8	3.358	3.417	2610	-4630
0.200	-3.7	3.383	3.440	2755	-5050

Eliminating e_{tj} between (7) and (10), replacing ϵ_{tj} by $\frac{1}{2}\epsilon_o$, as indicated by (27), and solving for S_{tj}

$$S_{tj} = \frac{E_j(e_{tr} - 0.5\epsilon_o) + \mu S_a}{1-\mu} \qquad (30)$$

where e_{tr} is given by (9). Also, from equations (12) and (13), in which axial strains are determined from Hooke's law,

$$e_{aj} = (1/E_j)(S_a - \nu\mu S_{tj})$$

$$e_{ar} = S_a/E_r$$

From equation (1),

$$t = \frac{Q}{S_a AC + l_r e_{ar} + l_j(e_{aj} + \epsilon_{aj})} \qquad (31)$$

ϵ_o (10^{-3})	e_{ar} (10^{-6})	e_{tr} (10^{-6})	S_{tj} (psi)	e_{aj} (10^{-6})	t (sec.)
0.050	-112	30.9	-1245	-538	35.5
0.063	-117	32.4	-1345	-560	37.1
0.080	-125	34.5	-1470	-592	39.5
0.100	-132	36.6	-1615	-622	41.9
0.126	-143	39.5	-1805	-666	45.3
0.159	-154	42.7	-2032	-710	48.9
0.200	-168	46.6	-2300	-764	53.4

where $\epsilon_{aj} = -\epsilon_o$, as indicated by (27).

The graph of plastic strain versus time (Fig. 18, curve marked "approx. 1") shows that the plastic strain rate is essentially constant at 8.5×10^{-6} sec^{-1}. It is less than the initially assumed rate of 4.66×10^{-5} sec^{-1}, and so the $s_o - \epsilon_o$ curve has to be lowered, for the second approximation, by a factor of

$$\text{antilog}\left[0.115 \log \frac{4.66 \times 10^{-5}}{8.5 \times 10^{-6}}\right] = 1.215$$

that is, the log S_o - log ϵ_o curve should be lower by log 1.215 = 0.085 than the one used in the first approximation. When this is done, and the above calculation is repeated, the ϵ_o - t curve (designated by "approx 2" in Fig. 18) shows the strain rate again to be essentially constant, this time at a level of 9.1×10^{-6} sec^{-1}. This is only 7 per cent different from the rate assumed initially for the second approximation, and the corresponding adjustment to S_o, for purposes of a third approximation, would be less than one per cent. Therefore, no further approximations are needed. The final results, extended to larger strains for purposes of comparison with the experimental results, are given in Table 5.

Full-Restraint Plastic Behavior - Measured versus Calculated

The test results for the thinnest joint, 0.020 in., are shown in Fig. 10. The results are expressed as load versus average strain over a 0.5-inch gage length straddling the joint, and so the calculated results have to be expressed in the same terms. Load is simply stress times area, and average strain depends on the strains in the steel and solder as follows.

$$(e_a)_{av} = \frac{\delta}{\ell} = \frac{\delta_r + \delta_j}{\ell_r + \ell_j} = \frac{\ell_r e_r + \ell_j (e_j + \epsilon_j)}{\ell_r + \ell_j} \qquad (32)$$

For the case at hand, test K-12, $l_r = 0.48$, $l_j = 0.02$, $A = 0.759$, and the values of e_r, e_j, and ϵ_j are given in Table 5. Substituting into equation (1) and plotting against load, we obtain the result shown in Fig. 19, where the experimental values are also shown for comparison. The results show that the measured plastic strain is smaller than the calculated plastic strain, that is, that the specimen is behaving plastically more stiff than the calculations would indicate. The effect is very small at the highest load, and large at the smaller loads. The difference is in the same direction as in the elastic case: the measured stiffness is a little greater than the calculated stiffness. In this case, however, the uncertainties connected with the fairing of the elastic line are higher, and such a strong conclusion cannot be drawn as for the elastic case.

ality ($R = S_{tj}/S_a$). From the theoretical analysis of the infinitesimally

ality ($R = S_{tj}/S_a$). From the theoretical analysis of the infinitesimally

thin solder joint, as presented in the preceding section, the triaxiality is found to be

ϵ_o (10^{-3})	S_a (psi)	S_{tj} (psi)	R
0.05	-2800	-1067	0.381
0.10	-3350	-1430	0.421
0.20	-4340	-2070	0.476
0.50	-6800	-3880	0.571
1.00	-10,070	-6640	0.658
2.00	-15,550	-11,800	0.760
4.00	-25,800	-21,950	0.850

The results are shown in Fig 20. A pronounced increase in triaxiality with increasing plastic strain is evident.

The triaxiality can also be determined from the experimental results by using the shear stress law, as given by equation (26).

$$S_o = S_{tj} - S_a$$

Dividing through by S_a, and solving for $R = S_{tj}/S_a$

$$R = \frac{S_{tj}}{S_a} = 1 + \frac{S_o}{S_a} \qquad (33)$$

Here, S_a is obtained from P in Fig. 10 by dividing by A = 0.759 and S_o is found from the appropriate curve in Fig. 17 and the plastic strain as determined from the plastic offset in Fig. 10. The plastic offset is the plastic component of average strain (averaged over the 0.5-inch gage length), which is related to the actual plastic strain in the solder by

$$(\epsilon_a)_{av} = \frac{\delta_{plastic}}{\ell} = \frac{\ell_j \epsilon_{aj}}{1/2} \qquad (34)$$

For the case at hand, where l_j = 0.02 inches

$$\epsilon_{aj} = \frac{(\epsilon_a)_{av}}{0.04} = (25) \times (\text{plastic offset}) \qquad (35)$$

Applying to the data in Fig. 10,

P (lb.)	Plastic Offset (10^{-3})	$\epsilon_{aj} = -\epsilon_o$ (10^{-6})	$\log \epsilon_o$	$\log S_o$	S_o (psi)	$\frac{S_{tj}}{S_a}$
8,000	0.020	-500	-3.301	3.462	2900	0.724
10,000	0.035	-875	-3.111	3.512	3250	0.756
12,000	0.045	-1125	-2.949	3.542	3480	0.780
14,000	0.065	-1625	-2.789	3.563	3630	0.803
16,000	0.080	-2000	-2.699	3.571	3730	0.823

These results are also plotted in Fig. 20, for comparison with the theoretical results. The fact that the measured stiffness is greater than the calculated stiffness, as noted before, is again evident, particularly at the smaller plastic strains.

Effect of Joint Thickness on Plastic Restraint

We have seen that the plastic restraint can be calculated for an infinitesimally thin joint, that is, where strain compatibility between the steel and solder completely restrains the solder from expanding transversely by any more than the steel does ("complete restraint"). We have also seen that the experimental restraint in the thinnest joint tested is at least as great as the theoretical restraint. From this observation, we must conclude that there was full restraint in the thinnest joint.

For longer joints there will presumably be less restraint than full restraint, and in such cases the amount of restraint would

be very difficult to determine theoretically. However, it can be determined rather easily by the same methods of analysis of the experimental data as in the preceding section. The values of load and plastic offset are obtained from Figs. 11 - 14. The other necessary data, including that for utilizing the data of Figs. 5 and 7, are:

Test Number	K-12	K-10	K-9	K-11	D-1
l_j (inches)	0.020	0.024	0.054	0.086	0.241
A ($in.^2$)	0.759	0.756	0.756	0.718	0.751
aging time (days)	0	27	3	5	6
de_{aj}/dt ($10^{-5} sec^{-1}$)	3.1	4.4	4.4	4.4	2.9
Strain Rate Correction*	1.000	1.040	1.040	1.040	1.000
Aging Correction	1.000	0.779	0.955	0.929	0.917
Overall Correction	1.000	0.809	0.993	0.965	0.917
Logarithm of Correction	zero	-0.092	-0.003	-0.016	-0.038

The results are shown in Fig. 21. The triaxiality values for each test are plotted versus the plastic strain values, on a logarithmic scale, to show the effects of plastic strain. The calculated values for an infinitesimally thin joint are also shown for comparison.

In all cases the triaxiality increases with plastic strain. For the longer joints the experimental curves have about the same slope as the theoretical curves at the smaller strains; but they tend to become less steep at the larger strains, that is, at large strains,

---

* Strictly speaking, the strain rate correction should be based on plastic strain rate, but since the correction was small, it was based on the elastic rate which is much more easily determined.

the restraint tends to build up less rapidly than theory would indicate. This effect might be due to the development of quite non-uniform strain along the axis ("barrelling").

The curves for the shorter joint are bunched. This is to be expected if full restraint prevails for all joint lengths up to a given value. From this bunching, we may conclude that the restraint does not diminish to appreciably less than full restraint until the joint length becomes greater than 0.054.

The curves for the shorter joints are invariably less steep than the theoretical curve, and are higher than the theoretical curve except at the largest strains. This behavior is consistent with that indicated by Fig. 20 for test K-12. At the smaller strains, the experimental values were less than the theoretical values. As noted above, no satisfactory explanation was found for this fact that the stiffness in the elastic region and at small plastic strains was greater than theory would indicate.

The effects described above are also evident in Fig. 22. where the axial stress is plotted against the logarithm of the plastic strain. The curves for the three shortest joints are bunched, and they lie above the theoretical curve for full restraint except at the largest strains. From these observations we may conclude that there was essentially full restraint in the three shortest joints.

The two dashed curves in Fig. 22 delineate the complete range between no restraint (uniaxial) and full restraint. The curve marked "uniaxial" is simply the plot of S_o versus $\log_{10} \epsilon_o$ from the theoretical

analysis of the infinitesimally thin joint. By comparing the experimental curves with the two limiting curves, it can be seen that the two longest joints represent degrees of restraint which are intermediate and small respectively.

The effects of joint thickness can be seen more directly if the curves of Figs. 21 and 22 are crossplotted. For this purpose, the abscissa will be joint-thickness-to-diameter ratio, as being a more basic quantity than joint thickness, since the law of similitude says the ratio is the governing quantity. The crossplotting has to be done at a particular value of plastic strain; 0.002 was selected arbitrarily for this purpose.

The results of the crossplotting are shown in Fig. 23. Note that as the joint becomes long, the triaxiality must approach zero and the axial stress must approach S_o. These limits are shown as dashed lines, marked "uniaxial". Also shown as a dashed line is the theoretical triaxiality for an infinitesimally thin joint. The line is shown as a short, horizontal line segment, because it is the asymptote that should be approached as the curve is extended to the left.

Fig. 23 shows that the experimental triaxialities become larger than the theoretical value for the shortest joint lengths, as we have seen before. With increasing joint length, the triaxiality decreases and becomes small in the neighborhood of a ratio of one, thus bearing out the predictions of St. Venant's principle. The curve of axial stress gives another indication of the same fact: the triaxiality becomes small at a joint-thickness-to-diameter ratio of unity.

The triaxiality curve in Fig. 23 is the essence of the results of this investigation. It is not as well-defined or as accurate as one might desire, but it is the only such curve available, as far as the author is aware. When used for engineering purposes, it might be well to scale down the ordinates in the ratio 0.76:0.84 in view of the fact that there cannot be more restraint than full restraint (the calculated triaxiality for an ideal, infinitesimally thin joint).

Composite Modulus

We consider now the elastic slopes of the load-deflection curves for the joint tests. Perhaps it would be more logical to consider the elastic behavior before the plastic behavior, since elastic strain precedes the onset of plastic flow, but a satisfactory analysis of the elastic slopes has to wait for an estimate of the amount of restraint, estimated from the plastic behavior, as we shall see.

From the initial slopes in Figs. 10 - 14, we can determine a "composite modulus", defined as the slope of a curve of axial stress versus the average strain over a $\frac{1}{2}$-inch gage length straddling the joint. For zero joint length the composite modulus will equal that of the steel, and for infinite joint length the composite modulus will equal that of the solder.

The subject of composite modulus is complicated by the fact that the value is affected by three factors: (1) joint length, as a fraction of the gage length; (2) restraint; (3) strain rate, which

affects the value of the modulus of the solder. In order to assess the relative importance of these three factors, let us examine the effect of each of the last two.

If there is no restraint, that is, if the stress is uniaxial, the composite modulus is

$$E_c = \frac{S_a}{(e_a)_{av}} = \frac{S_a}{\delta_a/\ell} = \frac{S_a \ell}{\delta_{ar} + \delta_{aj}}.$$

$$E_c = \frac{S_a \ell}{\ell_r e_{ar} + \ell_j e_{aj}} = \frac{S_a \ell}{\frac{S_a \ell_r}{E_r} + \frac{S_a \ell_j}{E_j}}$$

$$E_c = \frac{\ell}{\frac{\ell_r}{E_r} + \frac{\ell_j}{E_j}} \qquad (36)$$

If the steel has uniaxial stress, but the solder, being restrained by the steel from expanding as much as it normally would, has a triaxiality of $R = S_{tj}/S_a$, then e_{aj}, instead of being simply s_a/E_j, is

$$e_{aj} = \frac{S_a - \mu(S_{aj} + S_{tj})}{E_j} = \frac{S_a - 2\mu R S_a}{E_j}$$

from (13) and (33), and composite modulus is

$$E_c = \frac{\ell}{\frac{\ell_r}{E_r} + \frac{\ell_j}{E_j}(1 - 2\mu R)}$$

As we have observed previously, when there is full restraint, strain compatibility between the steel and solder results in a triaxiality in the solder of

$$R = \frac{S_{tj}}{S_a} = \frac{\mu}{1-\mu}\left(1 - \frac{E_j}{E_r}\right) \qquad (37)$$

and the composite modulus becomes

$$E_c = \frac{\ell}{\frac{\ell_r}{E_r} + \frac{\ell_j}{E_j}\left[1 - \frac{2\mu^2}{1-\mu}\left(1 - \frac{E_j}{E_r}\right)\right]}$$

as shown in equation (15).

Using equations (15) and (36) we find, for two strain rates and for the longest and shortest joints, that the composite moduli under full and no restraint are

Joint Length (in)	$\dot{e}_j$ (10^{-5} sec^{-1})	E_j (10^6 psi)	E_r (10^6 psi)	μ	Composite Modulus (10^6 psi)	
					Full Restraint	No Restraint
0.020	2.85	3.00	30.0	0.277	23.4	22.1
0.241	2.85	3.00	30.0	0.277	6.8	5.6
0.020	12.60	4.00	30.0	0.277	24.5	23.8
0.241	12.60	4.00	30.0	0.277	8.7	7.3

Note that neither strain rate nor restraint has a very large influence. We can see that the most important factor, by far, is the relative lengths of steel and solder making up the gage length, since this factor can cause the composite modulus to vary by a factor of ten, that is, from the 30 x 10^6 psi for steel to the approximately 3 x 10^6 psi for solder.

For the purpose of depicting the effect of the relative lengths of steel and solder, both theoretically and experimentally, it is desirable, for comparative purposes, that the theoretical values be for the actual strain rates and for the actual restraints that were present experimentally. This can be done in the case of strain rate, using the values from Table 4. The elastic restraint is not readily available, however, except for the triaxiality of 0.345 for full restraint, and so the elastic restraint will be taken as being proportional to the plastic restraint, shown in Fig. 23.

The results of the calculations are shown in Fig. 24. The measured values are consistently higher than the calculated values,

thus bearing out the previous conclusion for the case of full restraint, namely that the joint specimens are elastically stiffer than one would expect from theoretical analysis. The effects cannot be explained on the basis of errors resulting from the method of estimating the restraint, because the whole range of effects, from full restraint to none, is small. No explanation for this effect has been found.

Plastic Analysis of Thin Joint, with Residual Stress Considered

The solder and steel had coefficients of thermal expansion of $13 \times 10^{-6}\ {}^{o}F^{-1}$ and $6.5 \times 10^{-6}\ {}^{o}F^{-1}$, respectively. Because of this difference, the restrained cooling of the solder would produce transverse residual tensile stress in the joint. Since the specimen was free to move axially, no axial load would be developed. This analysis was made to determine the effect of residual transverse tensile stress on the strength of the joint.

For these conditions, the compatibility equation is

$$-\frac{\mu S_a}{E_r} = \frac{\Delta S_{tj}(1-\mu) - \mu S_a}{E_j} + \epsilon_{jt}$$

where,

$$\Delta S_{tj} = S_{tj} - R$$

and,

$$S_{tj} = S_{oj} + S_a$$

solving,

$$S_a = -\frac{\frac{\epsilon_o E_j}{2} + (S_{oj} - S_R)(1-\mu)}{1 - 2\mu + \mu(E_j/E_r)}$$

where S_R is the residual stress.

The axial stress was determined for the test conditions of joint K - 12 with $\epsilon_o = 1.75 \times 10^{-3}$, $\mu = 0.28$, $E_j = 1.85 \times 10^6$ psi, $E_r = 30 \times 10^6$ psi, $S_{oj} = 2900$ psi and $S_R = 2000$ psi. The value of S_R was estimated on the basis of age, relaxation and strain due to restrained cooling. For these conditions, the calculated axial stress was 6350 psi. For the same conditions, without residual stress, the calculated axial stress was 8120 psi.

Residual stress had a strong effect in weakening the joint. This effect, however, was in the wrong direction to account for the discrepancy between the previously calculated and experimental axial stress values.

Conclusions

1. The solder had a rate sensitivity of 0.115, where rate sensitivity is defined as the slope of the graph of log stress versus log plastic strain rate.

2. Cast solder lost hardness by aging. The decrease amounted to a 30 percent loss in yield strength in 80 days.

3. Modulus of elasticity of the solder increased with increasing strain rate. There was an increase in modulus by a factor of two with an increase in rate by a factor of ten.

4. For very thin joints, there was good agreement between the theoretical and experimental behavior in the plastic range, particularly at the larger strains.

5. Triaxiality in a thin joint increases from 0.345 in the elastic region to 0.76 at 0.002 plastic strain.

6. Plastic restraint, expressed as triaxiality at 0.002 plastic strain has its theoretical maximum up to a joint-thickness- to-diameter ratio of 0.03. Then it decreases and becomes quite small at a ratio of about unity.

7. The joint specimens were elastically more stiff than theory would indicate.

8. Tooling and techniques were developed for making high-quality solder joints.

Appendix 1

A Method for Determining the Stress State of Plastically Loaded Notched Bars

Sachs and Fried (1949) used an experimental method to determine the variation of axial strain with radius in a series of notched, cylindrical, steel tensile specimens. These specimens were loaded well into the plastic range, and the hardness distribution along the diameter of the minimum cross section was determined on a polished section. The longitudinal strains were determined from the hardness values by use of a hardness-strain calibration curve from a uniaxial tension test. The numerically largest principal plastic strain was taken as the criterion of strain hardening.

The known longitudinal strain distribution can now be used, together with the constant volume condition and the compatability condition, to obtain the tangential strain distribution by graphical integration:

$$\epsilon_r = -\epsilon_t - \epsilon_a$$

$$r \frac{d\epsilon_t}{dr} = \epsilon_r - \epsilon_t = -2\epsilon_t - \epsilon_a$$

for strains that are not too large.

Since all the strains are known, the effective strain, and hence the effective stress, S_o, can be determined. Now the Von Mises

condition and the equilibrium-of-force condition can be combined.

$$\frac{S_t - S_r}{\epsilon_t - \epsilon_r} = \frac{S_a - S_r}{\epsilon_a - \epsilon_r} = \frac{S_o}{\epsilon_a - \epsilon_r}$$

$$r \frac{dS_r}{dr} = S_t - S_r = S_o\left(\frac{\epsilon_t - \epsilon_r}{\epsilon_a - \epsilon_r}\right)$$

The radial, axial and tangential stress distributions can now be determined.

The above method was used on Sachs' data for a specimen, 2.58-inch-diam with a 0.516-inch profile radius, which fractured at a measured stress of 125,000 psi. The calculated average stress was 115,000 psi. This method is most satisfactory when all the strains are reasonably large, and loses accuracy when they become small, such as with severe triaxial restraint.

Appendix 2

Properties of Testing Machine Equipment

A Baldwin-Emery, type SR-4, 50,000 lb testing machine was used. The crosshead was screw-driven by an electronically-controlled, variable-speed motor through an adjustable-ratio gear box. The main SR-4 load system was supplemented by an auxiliary 500-lb load cell. The machine was equipped with a 2-inch-gage length SR-4 extensometer and load-strain recorder. In some tests, timing marks were made on the recorder by means of a Strobotac (see Fig. 25). A type F Huggenberger tensometer was also used for deformation measurement.

A machine speed control calibration and machine and fixture compliance measurements were made for use in strain rate determination. The calibration was found to be linear. The data is shown in Table 6. An elastic member, with known properties, was used in loading the equipment at a constant rate, and the machine drive deplacement, head displacement, and load were measured. Compliance, or the load rate of elastic deflection, was found for the machine and both test fixtures from the slope of the load-displacement plots. (See Fig. 26). The elastic deflection in the machine was determined by comparing, under load, the crosshead motion and the motion of the hand wheel on the

motor. The compliance data are given in Tables 7 and 8.

For a tensile load of 650 to 780-lb, the machine had a large drive displacement for a very small head displacement and increase in load. Plots of load and head displacement vs drive displacement illustrating this phenomenon are shown in Figs 26 and 27, respectively. This is due to clearance on the gear teeth of the rack and pinion for the lower head. The pinion supports the rack (and head) for tensile loads less than the head weight (about 700 pounds). For higher tensile loads, the pinion pulls down on the rack, but must turn a certain distance to do so, because of the clearance. On unloading the reverse is true; the pinion must turn freely for a certain time, as the load passes through the 700 pound range, before it can begin to "pick up" the head, thereby removing the weight of the head from the specimen. This "head pick-up effect" results in a drive displacement of about 4 revolutions of the handwheel without any head motion or load change. These 4 revolutions of drive displacement would cause 0.008 inches of unloaded head displacement at any load other than 700 pounds.

When the load reached the "head pick-up" range in a test made at some nominal strain rate, the test suddenly became a constant load test for a period, depending on machine speed, and then proceeded normally. In some early tensile tests on cast solder, this behavior produced a load-strain curve which seemed to have a yield point jog. Later test data taken in this load range have been adjusted to avoid the effects of the "head pick-up" discontinuity.

Appendix 3

Effect of Transverse Stress in the Steel Portions of the Joint Specimens

In the analysis of the joint specimens it was assumed that the transverse stress in the steel could be neglected. This assumption will now be examined is some detail.

It is known that the transverse stress in the steel cannot actually be zero, because of considerations of force equilibrium in the transverse direction. There will be transverse tensile stress in the steel to balance the transverse compressive stress in the solder. This transverse tension will be a maximum at the steel-solder interface and will die out nearly to zero, according to St. Venant's principal, in a distance from the interface equal to about one diameter. The dying-out effect will be approximately exponential.

The above facts can be expressed mathematically by the following relationship:

$$S_{tr} = S_{tr}^{o} e^{-\alpha x} \tag{38}$$

where S_{tr} is the transverse stress in the steel, x is axial distance from the steel-solder interface, e is the base of the natural logarithms, S_{tr}^{o} is the transverse stress at the interface (X = 0), and α is a constant that determines how fast the transverse stress decays. If we say that the transverse stress has decayed to one per cent at a distance equal to one diameter, then

$$S_{tr} = 0.01\, S_{tr}^{o} = S_{tr}^{o} e^{-\alpha x} \tag{39}$$

Since α for test K-12 is 0.983 in. (see Table 3), α is found to be 4.69.

The value of S_{tr}^{o} is governed by considerations of equilibrium of force in the transverse direction:

$$\int S_{tr}\, dA + \int S_{tj}\, dA = 0 \tag{40}$$

Our element of area (dA) is dx times the diameter, that is

$$dA = 0.983\, dx \tag{41}$$

Substituting into (40) and simplifying

$$\int S_{tr}\, dx + \int S_{tj}\, dx = 0 \tag{42}$$

The first integral in (42) covers the distance from the interface outward to infinity in both directions. The second integral covers the length of the solder joint; and since the transverse stress in the solder will be essentially uniform, the second integral may be replaced by $0.02\, S_{tj}$. Thus

$$2\int_{0}^{\infty} S_{tr}^{o} e^{-4.69x}\, dx + 0.02\, S_{tj} = 0 \tag{43}$$

from which S_{tr}^{o} is found to be $-0.0469\, S_{tj}$. Note that the transverse stress in the steel, even at its maximum, is only 5 percent of that in the solder.

Now the transverse stress distribution in the steel

$$S_{tr} = -0.0469\, S_{tj}\, e^{-4.69X} \tag{44}$$

can be used to correct the previous analysis in which this transverse stress was neglected. The compatibility condition applies at the interface (superscript zero), that is

$$e_{tr}^{\circ} = e_{tj} \tag{45}$$

Using Hooke's law to find e_{tr}°, and noting that the value desired is that at X = 0,

$$e_{tr}^{\circ} = \frac{S_{tr}^{\circ} - \mu(S_a + S_{tr}^{\circ})}{E_r} = \frac{S_{tr}^{\circ}(1-\mu) - \mu S_a}{E_r}$$

$$e_{tr}^{\circ} = \frac{-0.0469 S_{tj}(1-\mu) - \mu S_a}{E_r} \tag{46}$$

Similarly, by applying Hooke's law to the joint,

$$e_{tj} = \frac{S_{tj} - \mu(S_{tj} + S_a)}{E_j} = \frac{S_{tj}(1-\mu) - \mu S_a}{E_j} \tag{47}$$

Substituting (46) and (47) into (45) and solving for S_{tj},

$$S_{tj} = \frac{\mu S_a}{1-\mu}\left(\frac{E_r - E_j}{E_r + 0.0469 E_j}\right) \tag{48}$$

Note that, for $E_j = 3.05 \times 10^6$ and $E_r = 30.0 \times 10^6$, this expression gives

$$S_{tj} = 0.895\, \frac{\mu S_a}{1-\mu}$$

which is only 0.3 per cent different from the

$$S_{tj} = 0.898\, \frac{\mu S_a}{1-\mu}$$

for negligible transverse stress in the steel.

Now the composite modulus, for the more rigorous case being

considered here, can be determined

$$E_c = \frac{S_a}{(e_a)_{av}} = \frac{S_a}{(\delta_a/l)} = \frac{S_a l}{\delta_a} = \frac{S_a l}{\delta_{ar} + \delta_{aj}} \tag{49}$$

The deflections, δ_{ar} and δ_{aj}, are found from the axial strains, which are given by Hooke's law.

$$e_{ar} = \frac{S_a - \mu(S_{tr} + S_{tr})}{E_r} = \frac{S_a - 2\mu S_{tr}}{E_r} \tag{50}$$

$$e_{aj} = \frac{S_a - \mu(S_{tj} + S_{tj})}{E_j} = \frac{S_a - 2\mu S_{tj}}{E_j} \tag{51}$$

The steel deflection, for a gage length straddling the joint with the joint centered, will consist of two parts, each extending from the steel-solder interface to the gage mark, namely a distance equal to half the length of steel (l_r). Mathematically speaking

$$\delta_{ar} = 2\int_0^{0.5 l_r} e_{ar}\, dy \tag{52}$$

Substituting (44) into (50) and the result into (52) and evaluating the integral,

$$\delta_{ar} = \frac{l_r S_a}{E_r} + \frac{0.04\mu S_{tj}}{E_r}\left(1 - e^{-2.345 l_r}\right) \tag{53}$$

The solder deflection is simply the joint length times the solder strain, or

$$\delta_{aj} = \frac{l_j S_a}{E_j} - \frac{2 l_j \mu S_{tj}}{E_j} \tag{54}$$

Substituting (53) and (54) into (49) and replacing S_{tj} by its value in (48), the composite modulus is found to be 23.0×10^6 psi, which

is very little different from the 23.5×10^6 psi which was found more easily by neglecting the transverse stress in the steel.

Appendix 4

Consideration of Uniaxiality Assumption in the Calculation of Elastic Strain Rates

In the analysis of elastic strain rate for the joint tests, the stress was considered uniaxial in both steel and solder. In this case

$$e_{aj} = \frac{S_a}{E_j} = \frac{P}{AE_j}$$

according to equation (4), and the corresponding strain rate, according to equation (6), is

$$\frac{de_j}{dt} = \frac{Q}{AE_jC + \ell_r(E_j/E_r) + \ell_j}$$

We shall now examine whether this assumption is good enough for our purposes.

We have seen (Appendix 3) that the transverse stress in the steel is small, even at the steel-solder interface, and that it dies off rapidly with axial distance from the interface. Consequently, we would not expect the assumption of uniaxiality in the steel to cause a serious error. By contrast, we know that there is considerable transverse stress in the solder under conditions of full restraint. Equation (37) shows the triaxiality to be

$$R = \frac{S_{ej}}{S_a} = \frac{\mu}{1-\mu}\left(1 - \frac{E_j}{E_r}\right)$$

This amounts to 0.345 for $E_j = 3 \times 10^6$, and this cannot be disregarded without proper justification. Consequently, we shall now compare

elastic strain rate, and the corresponding composite modulus, for both full restraint and no restraint, in the case of one particular test, K-12.

For full restraint, the axial strain in the solder, instead of being the expression indicated by equation (4), is

$$e_{aj} = \frac{S_a - \nu_j S_{tj}}{E_j} = \frac{S_a - \frac{\nu_j^2 S_a}{1-\nu}\left(1 - \frac{E_j}{E_s}\right)}{E_j} = \frac{P}{AE_j}\left[1 - \frac{\nu_j^2}{1-\nu}\left(1 - \frac{E_j}{E_s}\right)\right] \quad (55)$$

Equations (4) and (55) differ by the quantity in brackets in equation (55), which amounts to 0.809 for $E_j = 3 \times 10^6$, or 19 percent less than the value for the uniaxial case. Now if (55), instead of (4), is substituted into (3) and the equation is simplified in the same manner as before, we find the expression for strain rate to be

$$\frac{de_j}{dt} = \frac{Q}{\left[l_j + \frac{E_j(cA + l_s/E_s)}{1 - \frac{\nu_j^2}{1-\nu}(1 - E_j/E_s)}\right]} \quad (56)$$

instead of the expression indicated by equation (6). When this is solved graphically by the same method as before, we obtain the dotted, instead of the dashed, line in Fig. 28, which gives $E_j = 2.9 \times 10^6$ psi and $de_j/dt = 2.6 \times 10^{-5}\ sec^{-1}$ instead of the previous result of $E_j = 3.05 \times 10^6$ psi and $de_j/dt = 3.1 \times 10^{-5}\ sec^{-1}$.

Now let us see what effect these differences have on the composite modulus. We have seen that the composite modulus for full restraint is given by equation (15) as

$$E_c = \frac{l}{\frac{l_r}{E_r} + \frac{l_j}{E_j}\left[1 - \frac{2\mu^2}{1-\mu}\left(1 + \frac{E_j}{E_r}\right)\right]}$$

For test K-12, $l_r = 0.48$, $l_j = 0.02$, $E_r = 30 \times 10^6$, $\mu = 0.277$, $l = 0.50$, and we are interested in the effect of a difference in E_j between 2.9 and 3.05. Substituting:

E_j	$1 - \frac{E_j}{E_r}$	bracket quantity	$\left(\frac{l_j}{E_j}\right)$(bracket)	Denominator	E_c
3.05×10^6	0.898	0.8095	0.00530×10^{-6}	0.02130×10^{-6}	23.5×10^6
2.9×10^6	0.903	0.8085	0.00557×10^{-6}	0.02157×10^{-6}	23.2×10^6

The difference is small enough for our purposes.

Selected Bibliography

Bridgman, P. W., 1944, The stress distribution at the neck of a tension specimen: Trans. Am. Society for Metals, v. 32, p. 553.

Fiftal, C. E., 1967, Dynamic deformation of copper: Master's Thesis T-1141, Colorado School of Mines.

Hiers, G. O., and Schumacher, E. E., 1948, Soldering with soft solders: Metals Handbook, 1949 Ed., Am. Society for Metals, Cleveland, Ohio, p. 81.

Houidobre, R. A., 1965, Analytical and experimental plastic strain profiles in high velocity impact: Doctoral Dissertation T-1024, Colorado School of Mines.

Lubahn, J. D., 1947, Notch tensile testing, Fracturing of metals: Am. Society for Metals, Cleveland, Ohio, p. 129.

Lubahn, J. D., Culver, R. S., and Straw, R. L., 1965, Effect of strain rate on flow stress of copper: Colorado School of Mines research Report for Kirtland Air Force Base, March 17, 1965.

Neuber, H., 1937, Theory of notch stresses. Principles for exact stress calculation: Julius Springer, Berlin. Translated by F. A. Brown, David Taylor Model Basin, Washington, D. C., November 1965.

Orowan, E., 1946, Notch brittleness and the strength of metals: Institution of Engineers and Shipbuilders in Scotland, Trans., v. 89, p. 165-204.

Parker, E. R., Davis, H. E., and Flanigan, A. E., 1946, A study of the tension test: Proc. A S T M, v. 89, p. 1159.

Peterson, R. E., 1953, Stress concentration design factors: John Wiley and Sons, New York, and Chapman and Hall, London.

Sachs, G., and Fried, M. L., 1949, Notch bar tension tests on annealed carbon steel specimens of various sizes and contours: Symposium on Deformation of Metals as Related to Forming and Service, A S T M Special Technical Publication No. 87.

United States Steel Co., 1957, The making, shaping and treating of steel, 7th Ed.: United States Steel Co., Pittsburgh, Pennsylvania, p. 644.

Table 1

Rate-Change Data for Cast Solder

Test No.	Initial Condition (Age and percent strain)	Machine Speed (mil/min)	Plastic Strain (percent)	Strength (psi)
C-4-2	Cast 62 da + 0.5	5	0.7	3120
C-4-3	1.2 + 16 hr	5	1.3	2970
		5	1.9	3220
		15	1.9	3890
C-4-4	3.1 + 0.5 hr	5	3.3	3290
		5	3.4	3510
		15	3.4	3900
		15	3.8	3950
		28	3.8	4200
C-4-5	4.1 + 0.5 hr	5	4.3	3450
		5	4.4	3480
		41.5	4.4	4250
C-4-6	14.5	5	14.7	3020
		5	15.0	3480
		72	15.0	4860

Table 2

Yield Strength and Knoop Hardness for

Cast Solder of Various Ages

Test No.	Age (days)	*Yield Strength (psi)	Knoop Diam (mu at 100 g)
C-3	79	3270	324
C-7	66	3090	322
C-12	10	3960	302
C-13	0.1	4500	294

* at head speed of 12.5 mil/min

Table 3

Joint Test Conditions

Specimen No.	Joint Length (in.)	Joint Diam (in.)	Joint Area (sq in)	Specimen Length (in.)	Reduced Section (in.)	Testing Speed (mil/min)	Age Days
K- 12	0.020±0.004	0.983	0.759	2.38	1.50	5	0
K - 10	0.024±0.003	0.982	0.756	2.41	0.78	8	27
K - 9	0.054±0.005	0.982	0.756	2.48	0.72	8	3
K - 11	0.086±0.005	0.956	0.718	2.50	1.00	8	5
D - 1	0.241-0.006	0.978	0.751	2.60	0.88	5	6

Table 4

Elastic Strain Rates

Test	K - 12	K - 10	K - 9	K - 11	D - 1
A (in^2)	0.759	0.756	0.756	0.718	0.751
Q(10^{-5} in/sec)	8.33	13.3	13.3	13.3	8.33
1_j (in)	0.020	0.024	0.054	0.086	0.241
1_r (in)	2.36	2.39	2.43	2.41	2.36
E_j (10^6 psi)	3.05	3.35	3.35	3.35	3.00
$\frac{de_j}{dt}$(10^{-5} sec^{-1})	3.1	4.4	4.4	4.4	2.9

Table 5

Stresses and Strains in Joint Test Specimen K - 12

$\epsilon_o = -\epsilon_{aj}$ (10^{-3})	S_o (psi)	$-S_a$ (psi)	$-S_{tj}$ (psi)	$-e_{ar}$ (10^{-6})	$-e_{aj}$ (10^{-6})	P (lb)
0.05	1,730	2,800	1,067	93	446	2,120
0.10	1,940	3,350	1,430	112	517	2,540
0.20	2,270	4,340	2,070	145	646	3,290
0.50	2,900	6,800	3,880	227	940	5,160
1.00	3,410	10,070	6,640	336	1,292	7,650
2.00	3,730	15,550	11,800	518	1,825	11,800
4.00	3,870	25,800	21,950	860	2,762	19,600

Table 6

Baldwin Machine Speed Settings - Gears T & R

(Speed in mil/sec of unloaded crosshead)

Dial No.	Speed	Dial No.	Speed
5	0.042	20	0.691
6	0.083	23.5	0.934
7	0.133	30	1.20
9	0.208	35	1.40
9.5	0.234	52	2.10
10	0.250	69	2.80
15	0.466	90	3.65

Table 7

Compliance Values of Testing Machine

Load Cell	Load Range (lb)	Compliance (10^{-6} in/lb)
Auxiliary	20 - 100	24.6
Auxiliary	100 - 500	13.4
Standard	0 - 650	0.77
Standard	750 - 1,300	3.95
Standard	1,500 - 45,000	1.03

Table 8

Compliance Values of Machine Fixtures

Fixture	Compliance (10^{-6} in/lb)
Button-head, tensile	5.44
Spherical, compression	0.016

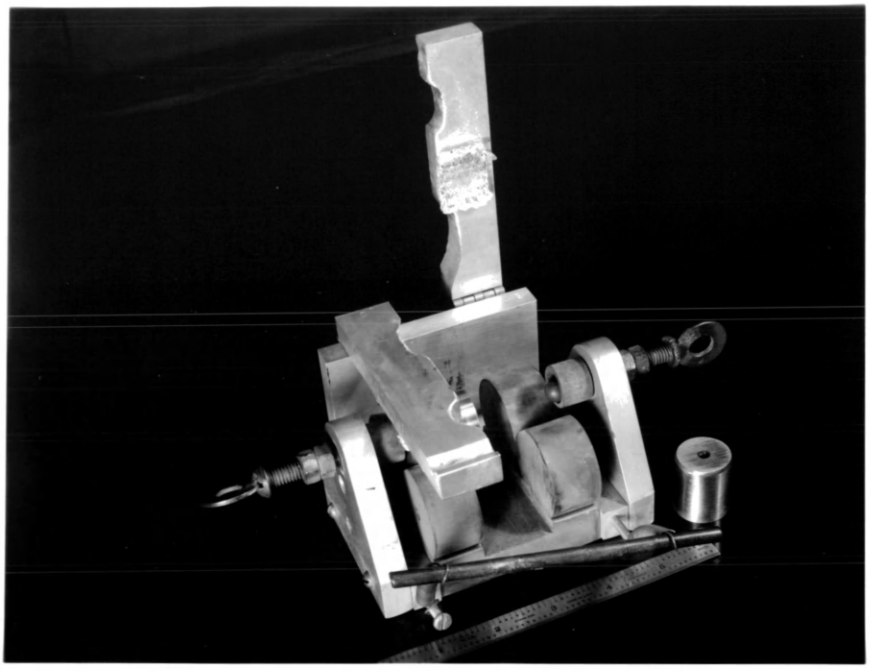

Figure 1. Support Fixture with Specimen Bars

Figure 2. Joint Mold with Seals

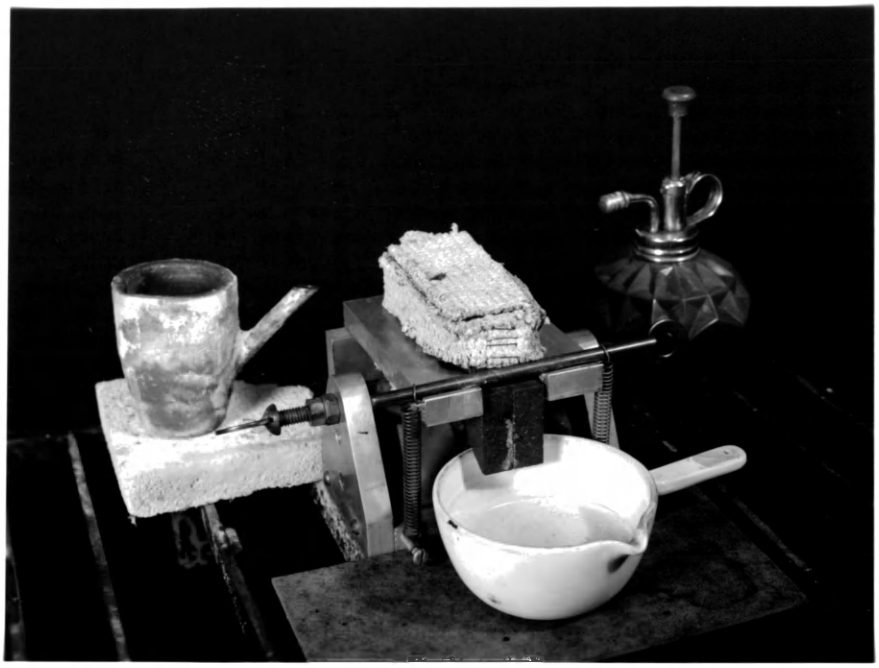

Figure 3. Assembled Mold and Fixture

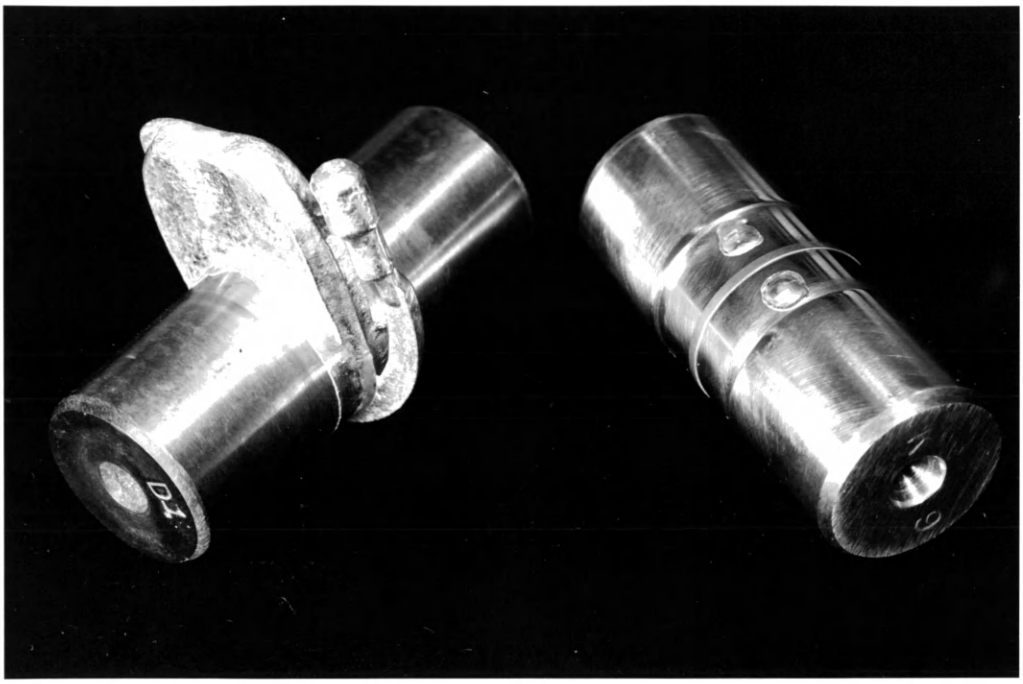

Figure 4. Joint Specimens As-Cast and As-Prepared

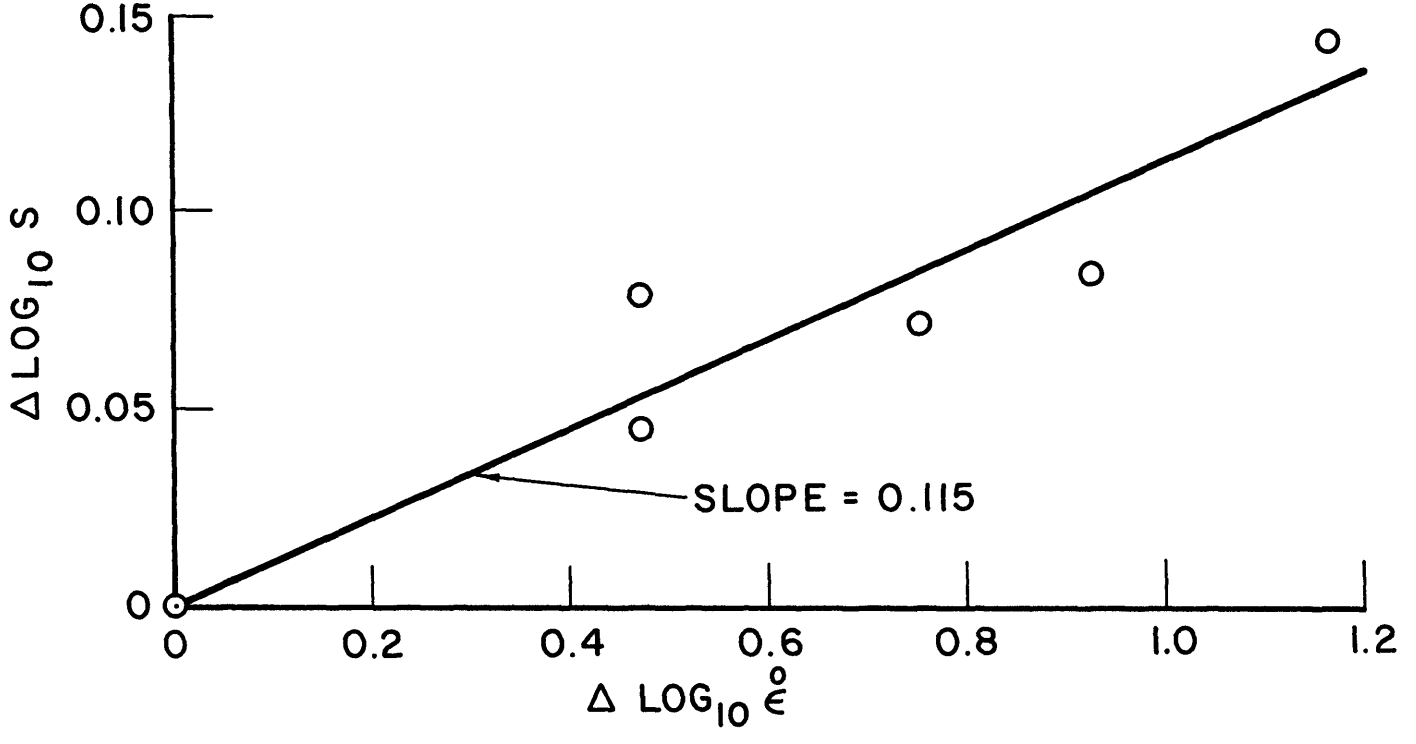

FIGURE 5. STRAIN-RATE SENSITIVITY

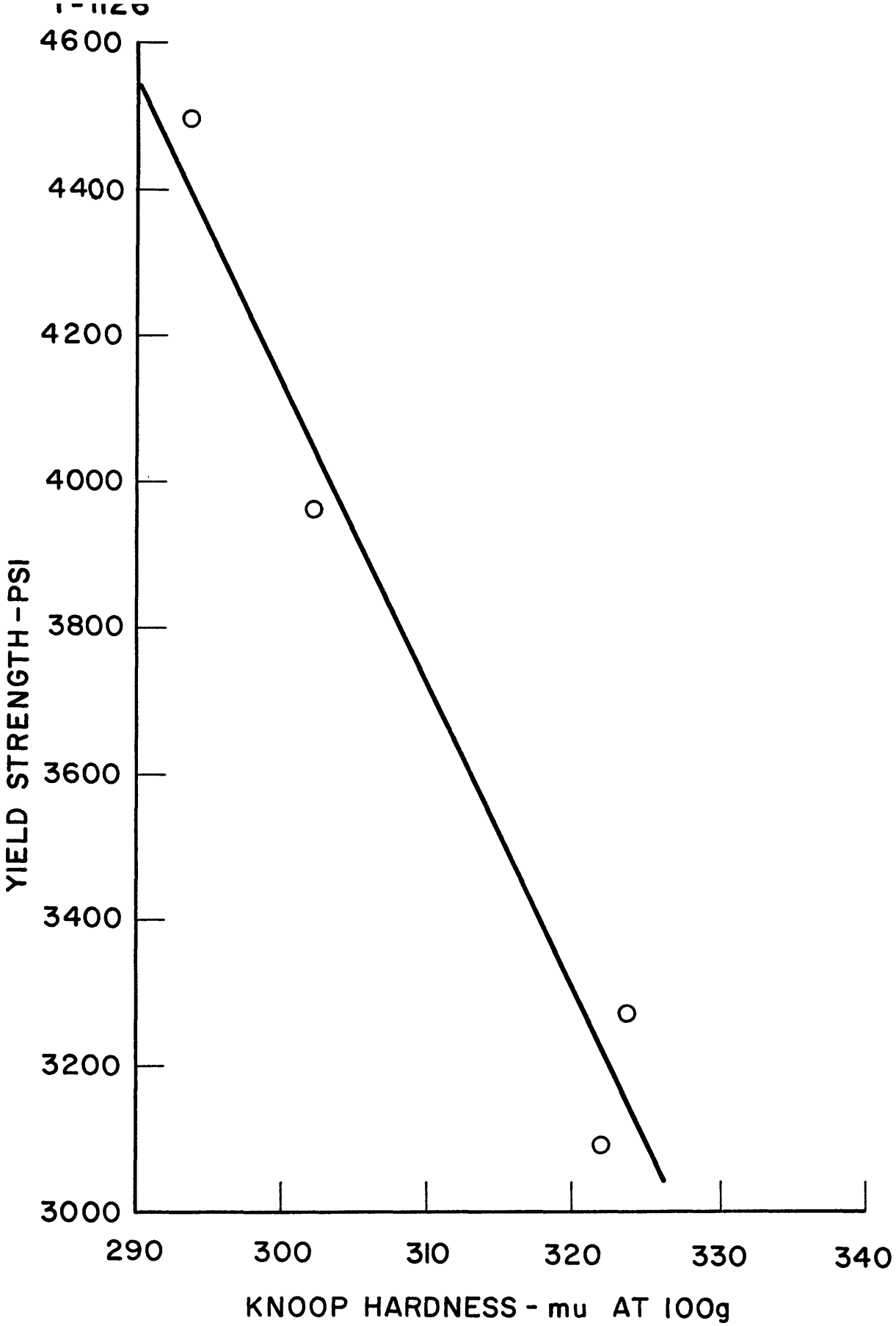

FIGURE 6. HARDNESS - YIELD STRENGTH RELATIONSHIP FOR CAST-AND-AGED SOLDER. UNLOADED CROSSHEAD SPEED: 12.5 MILS/MIN

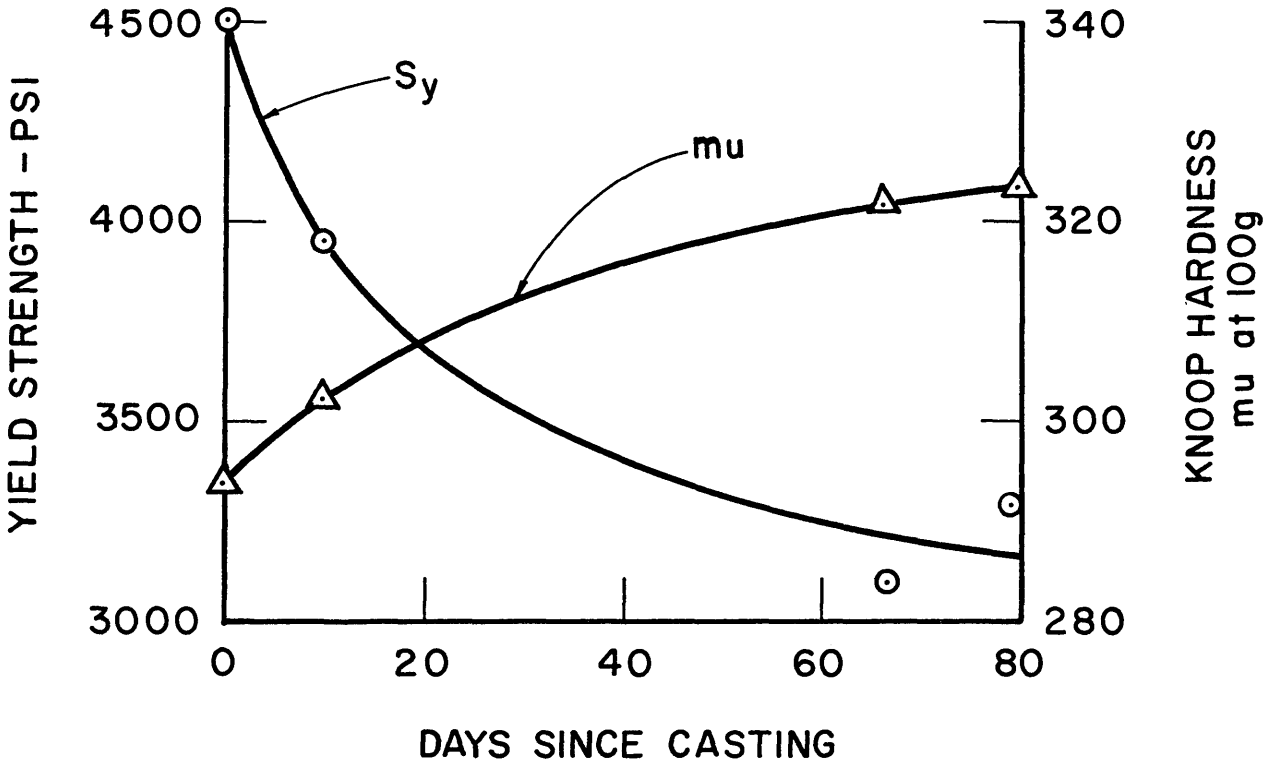

FIGURE 7. EFFECT OF AGING ON YIELD STRENGTH AND HARDNESS-UNLOADED CROSSHEAD SPEED: 12.5 MILS / MIN

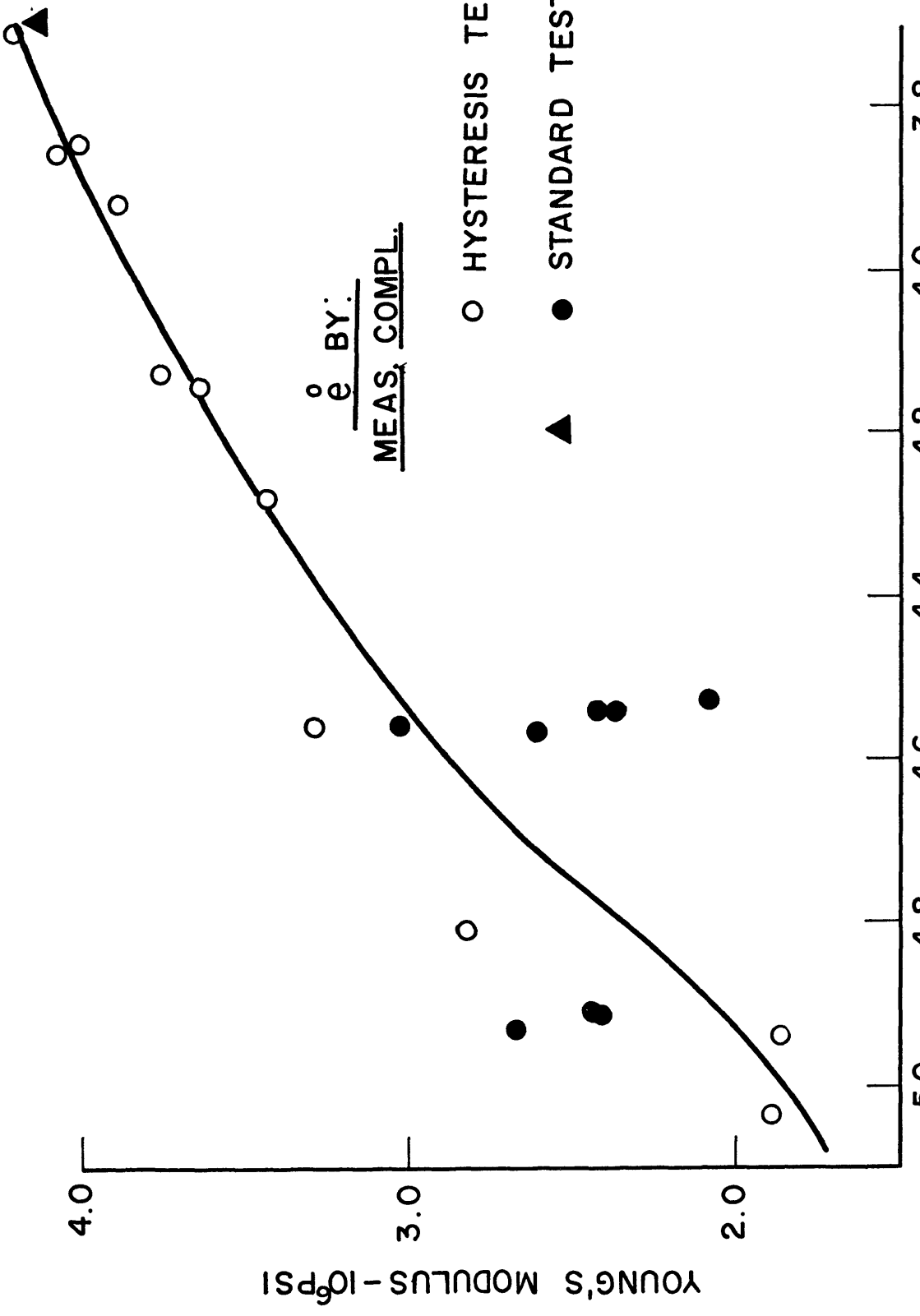

FIGURE 8. EFFECT OF STRAIN-RATE ON YOUNG'S MODULUS

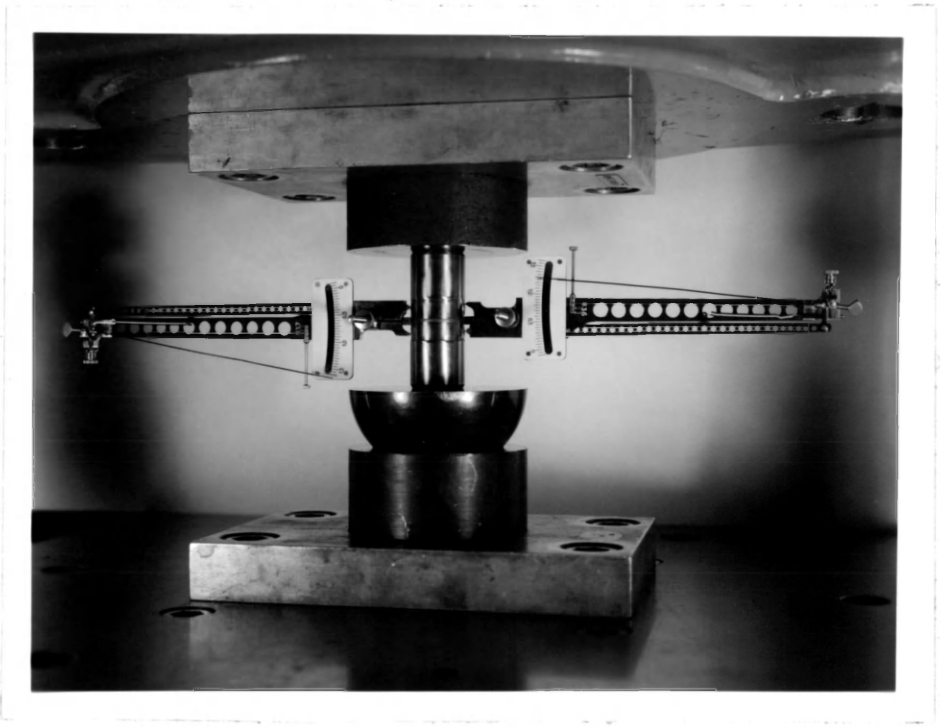

Figure 9. Testing of Joint

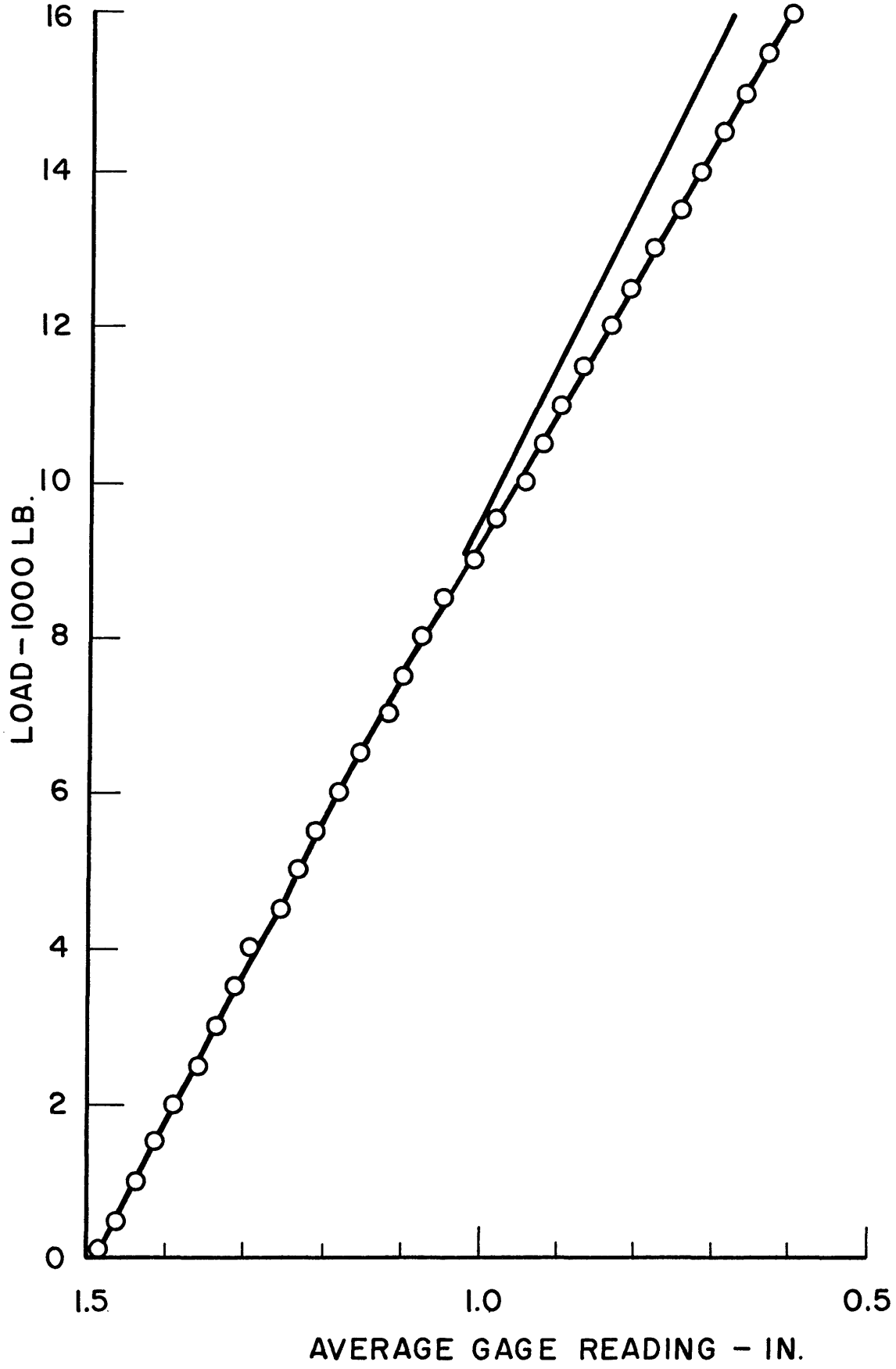

FIGURE 10. JOINT COMPRESSION TEST K-12

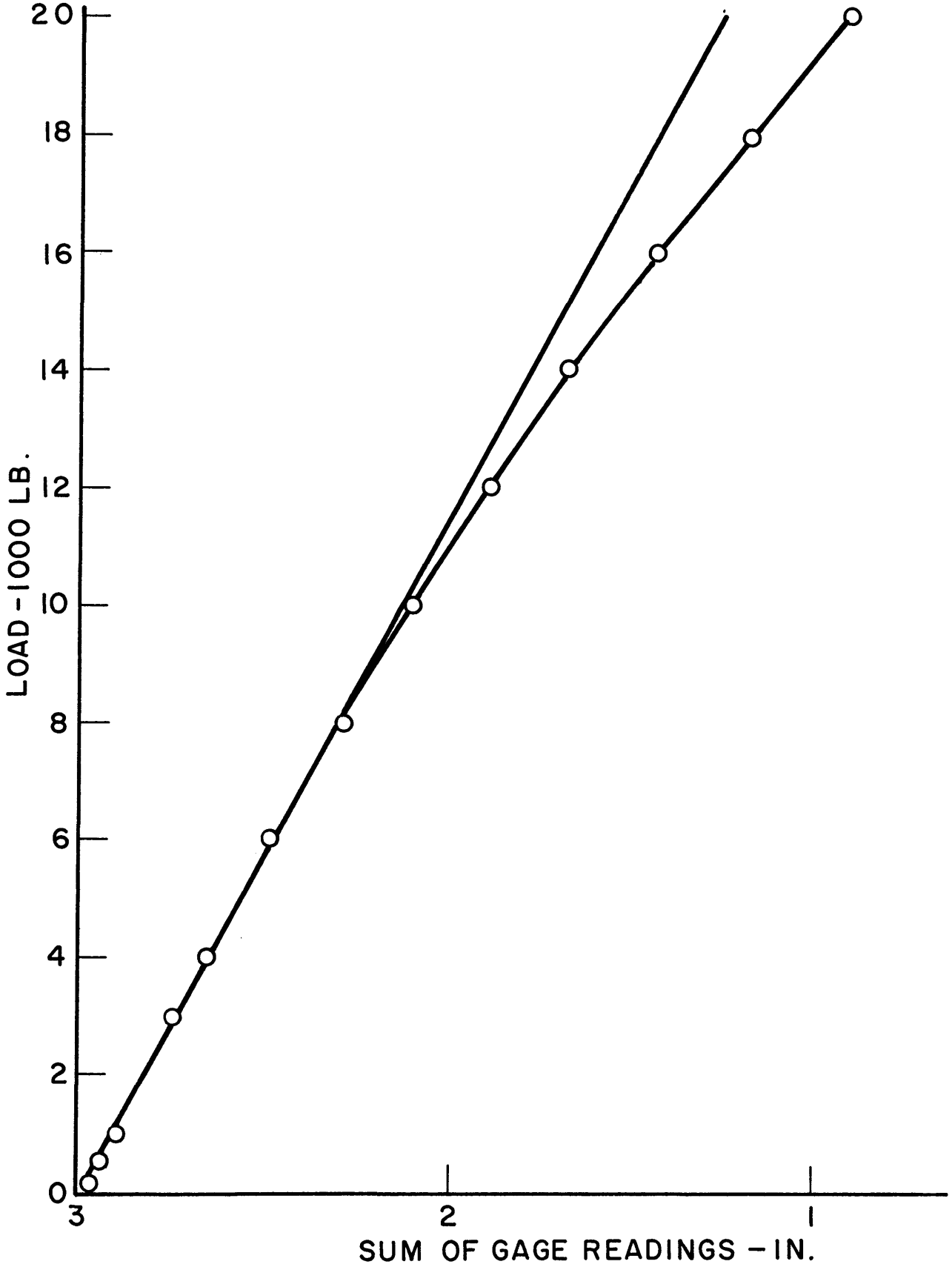

FIGURE 11. JOINT COMPRESSION TEST
K-10

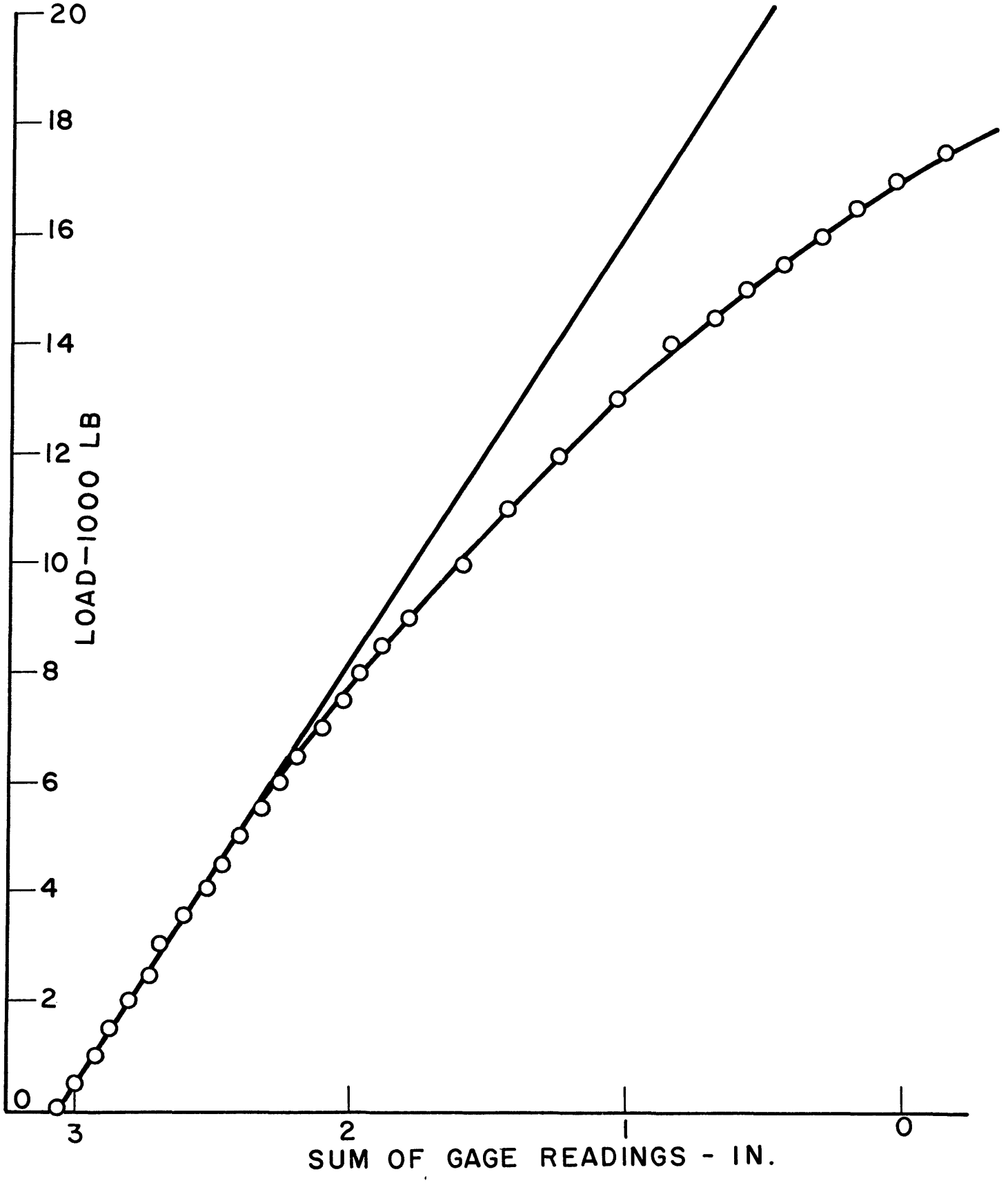

FIGURE 12. JOINT COMPRESSION TEST K-9

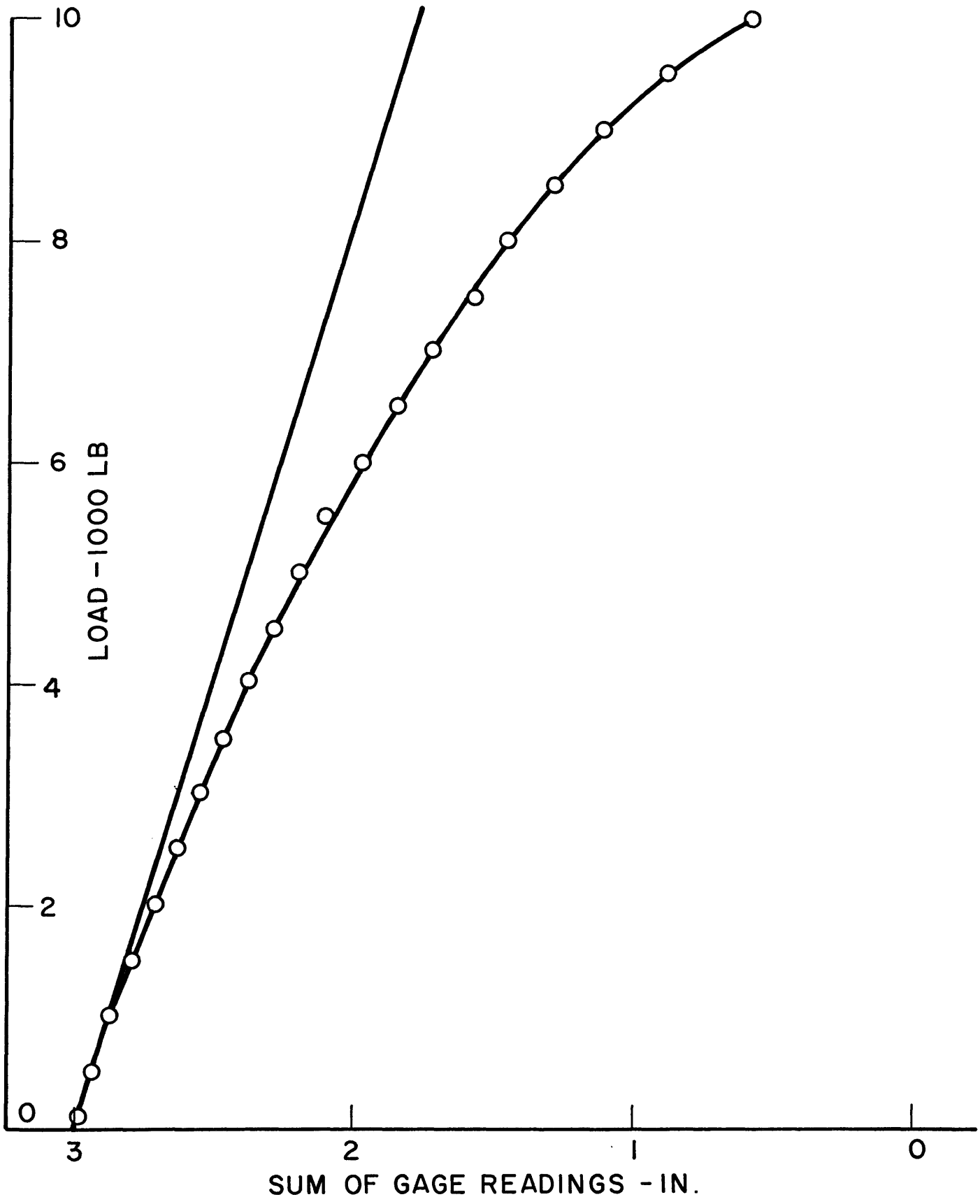

FIGURE 13. JOINT COMPRESSION TEST K-11

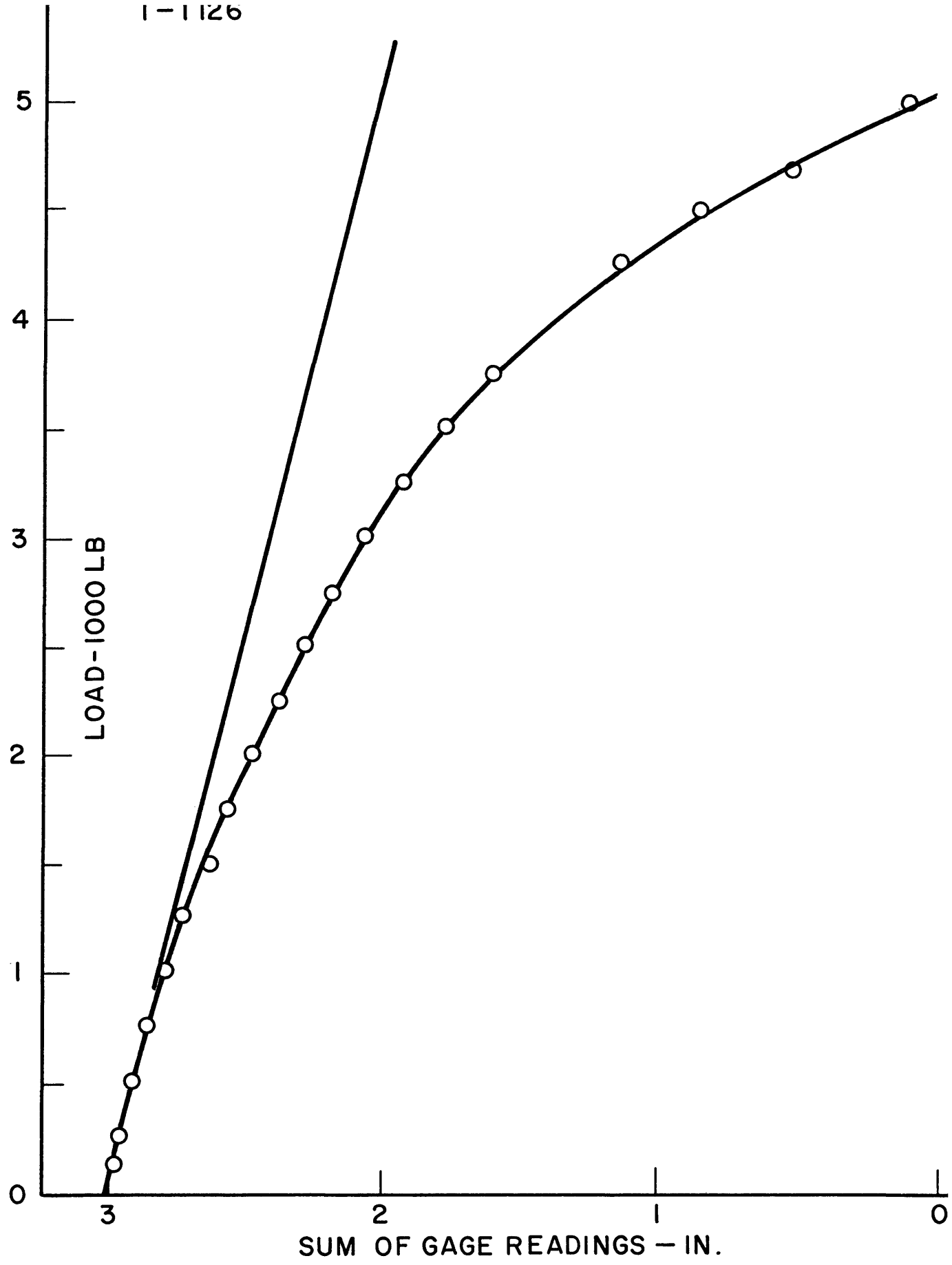

FIGURE 14. JOINT COMPRESSION TEST SPECIMEN D-1

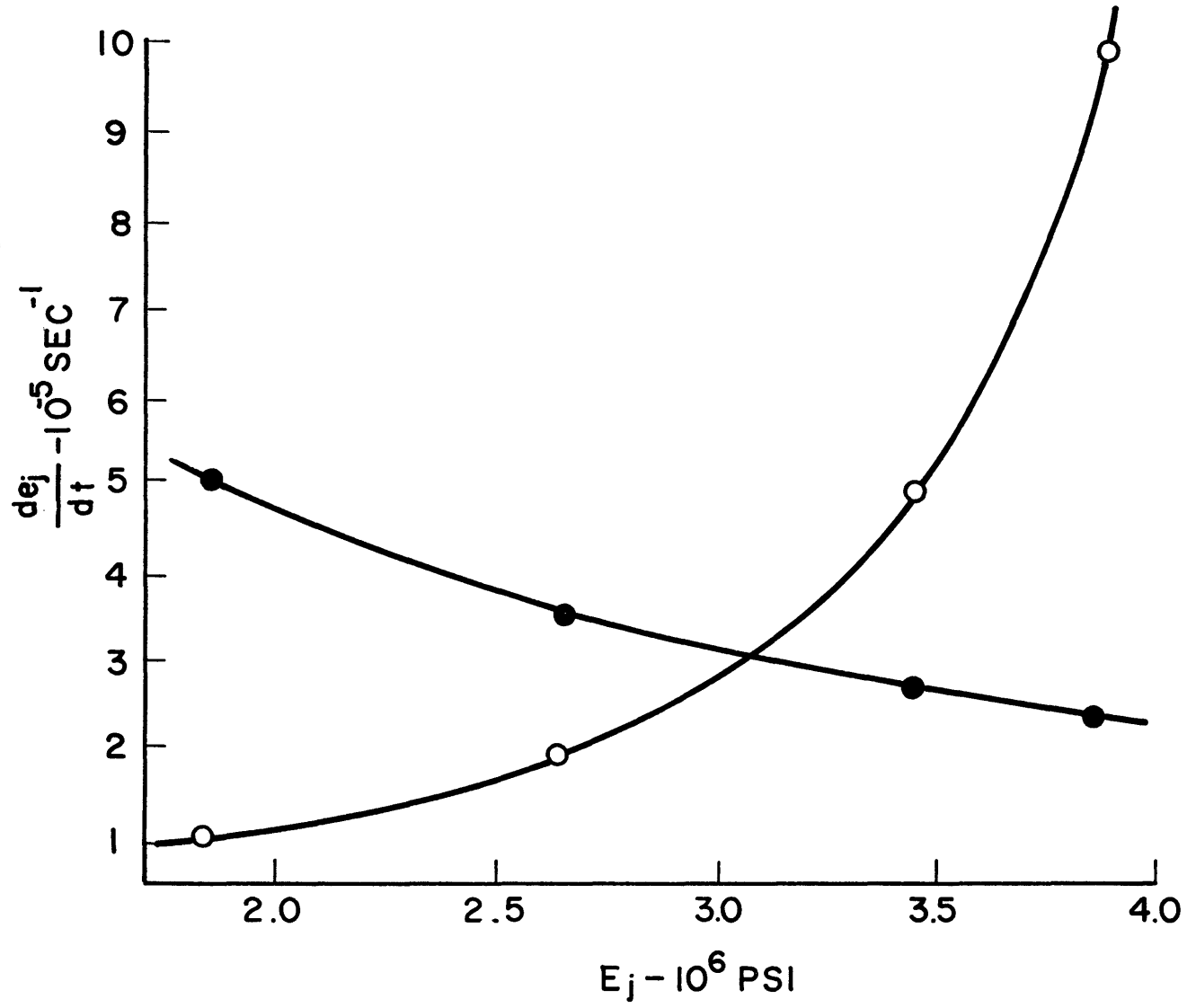

FIGURE 15. GRAPHICAL DETERMINATION OF ELASTIC STRAIN RATE IN TEST K-12

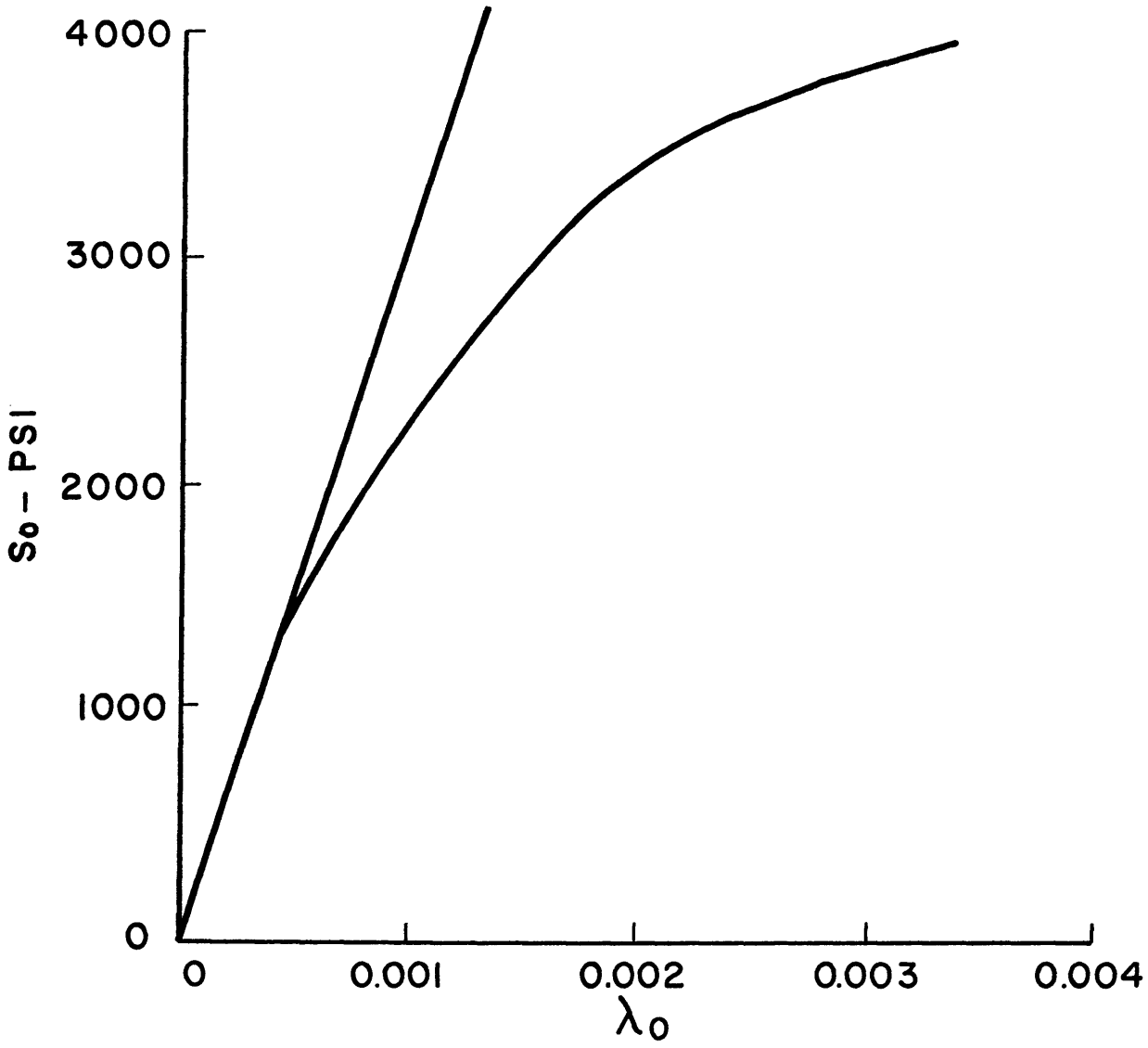

FIGURE 16. STRESS-STRAIN IN UNIAXIAL TENSION FOR BUTTON-HEAD SOLDER SPECIMEN C-12

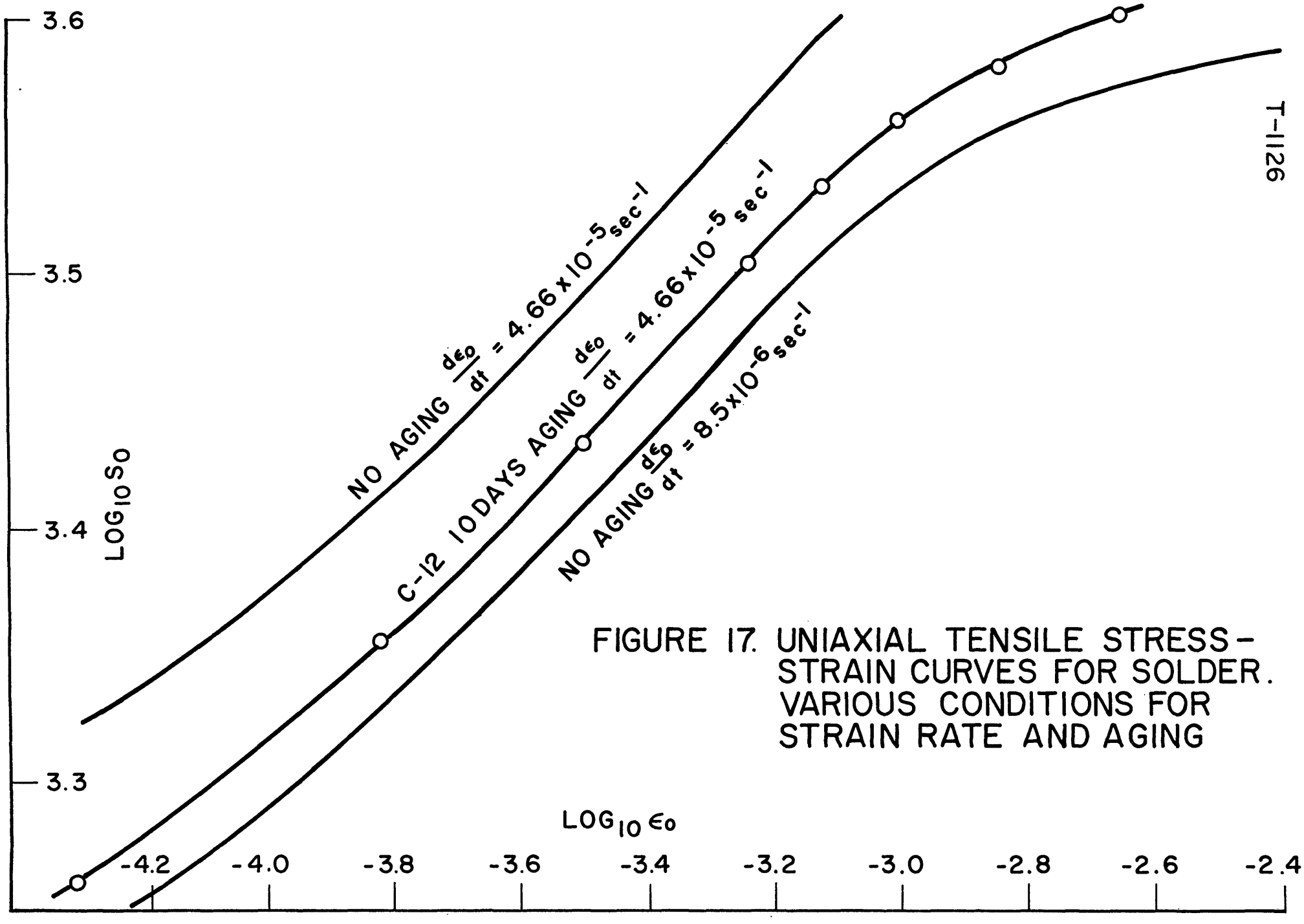

FIGURE 17. UNIAXIAL TENSILE STRESS-STRAIN CURVES FOR SOLDER. VARIOUS CONDITIONS FOR STRAIN RATE AND AGING

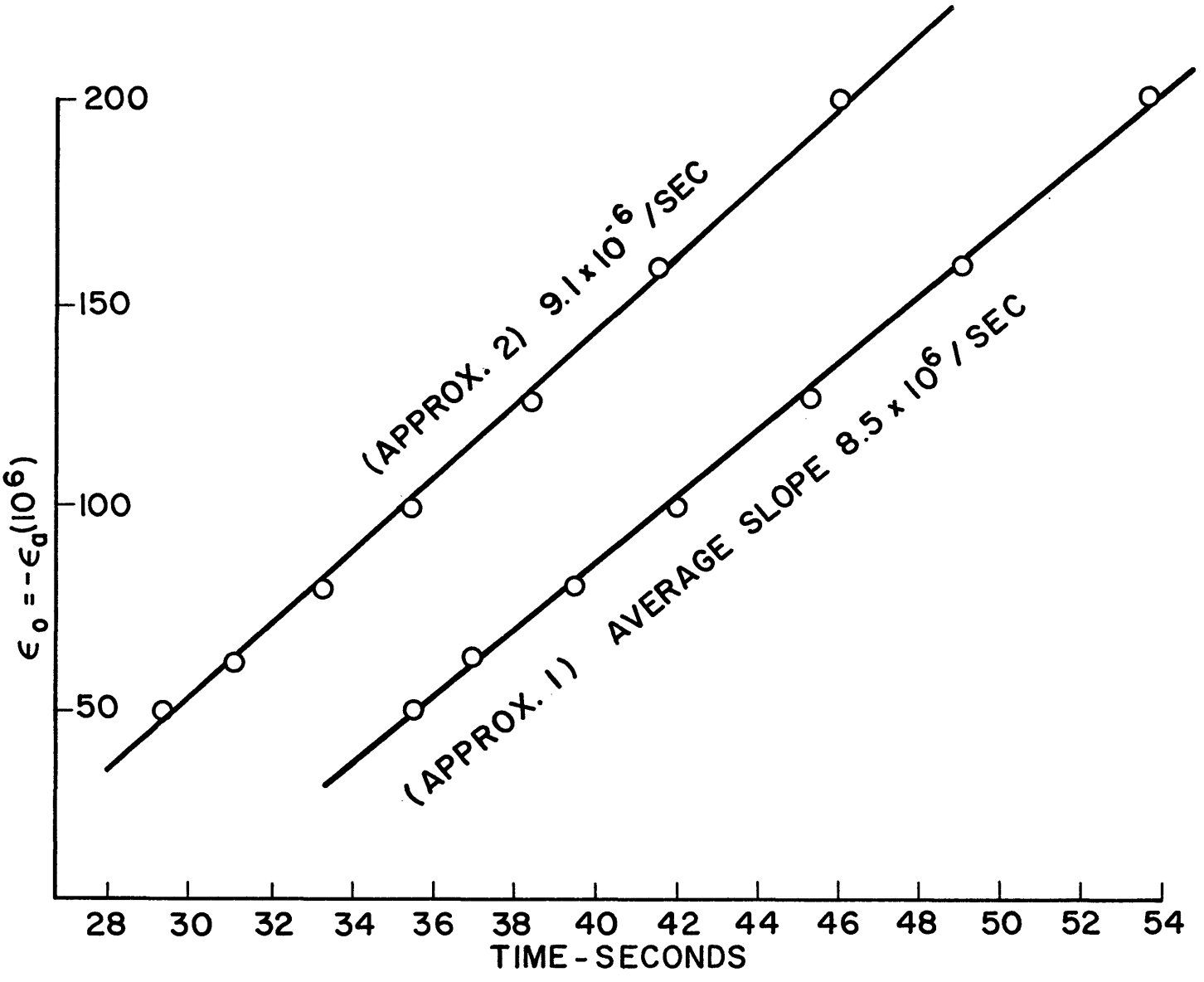

FIGURE 18. GRAPHICAL DETERMINATION OF PLASTIC STRAIN RATE TEST K-12

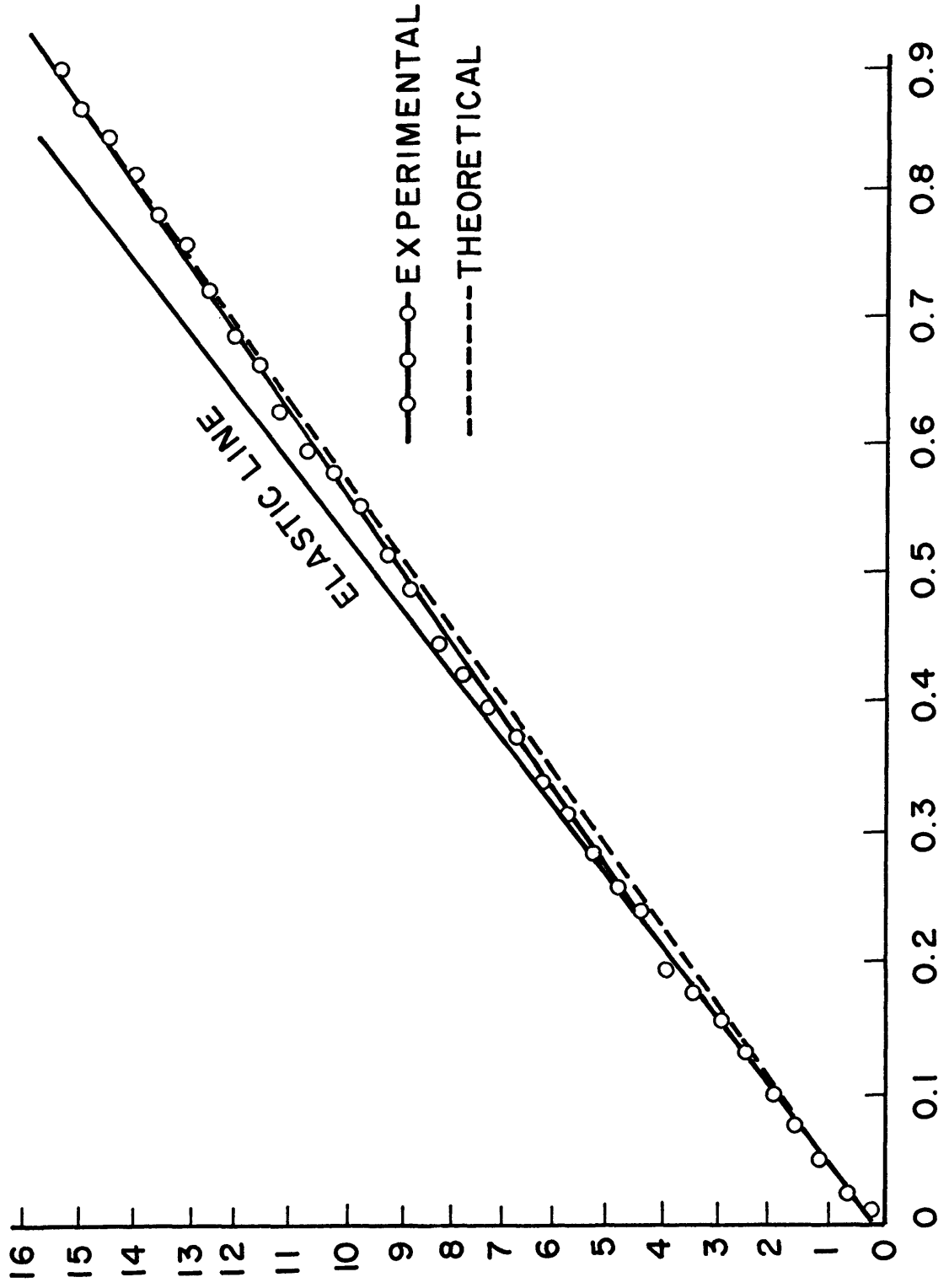

FIGURE 19. EXPERIMENTAL AND THEORETICAL LOAD-DEFLECTION

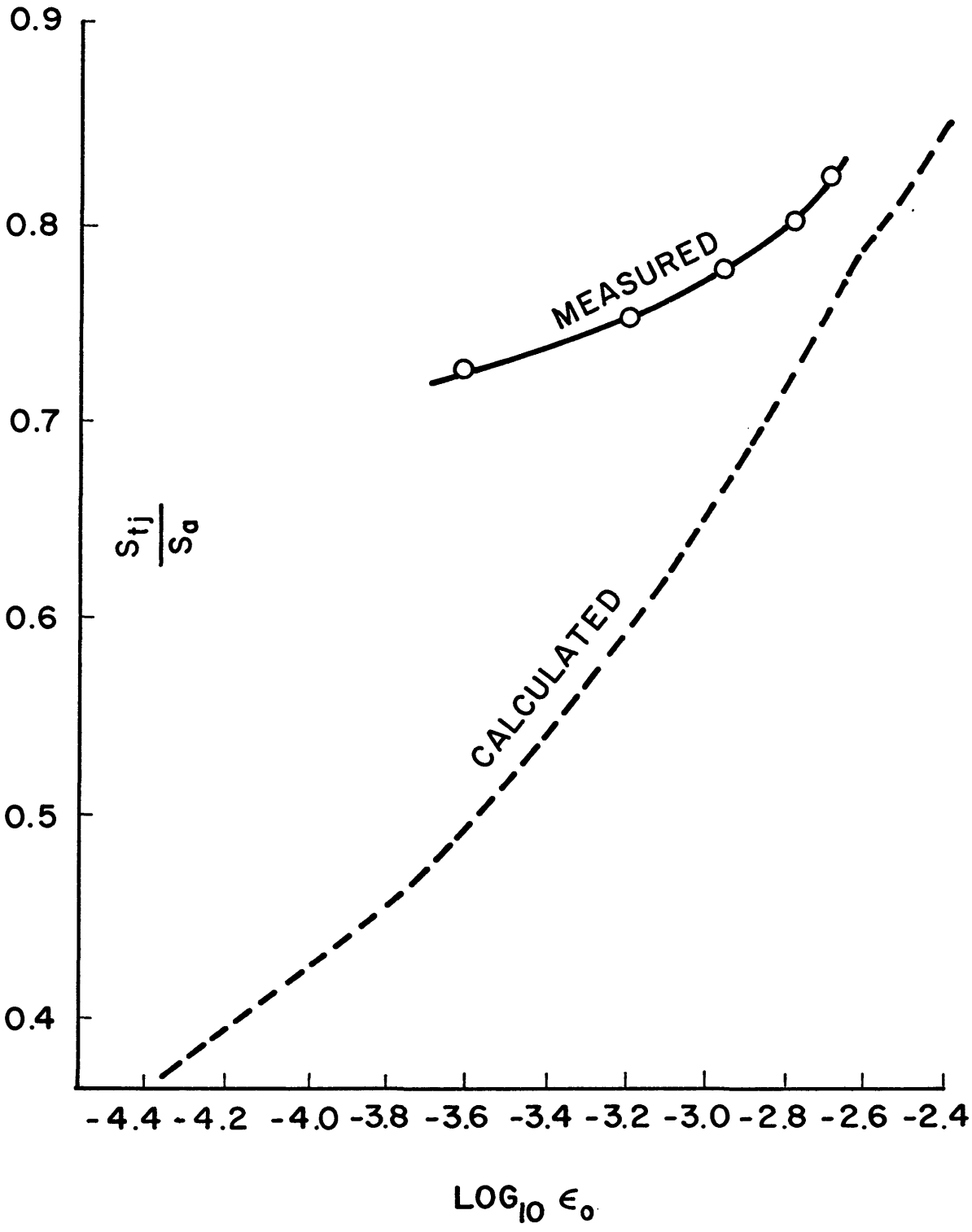

FIGURE 20. PLASTIC TRIAXIALITY IN THE THINNEST JOINT (TEST K-12)

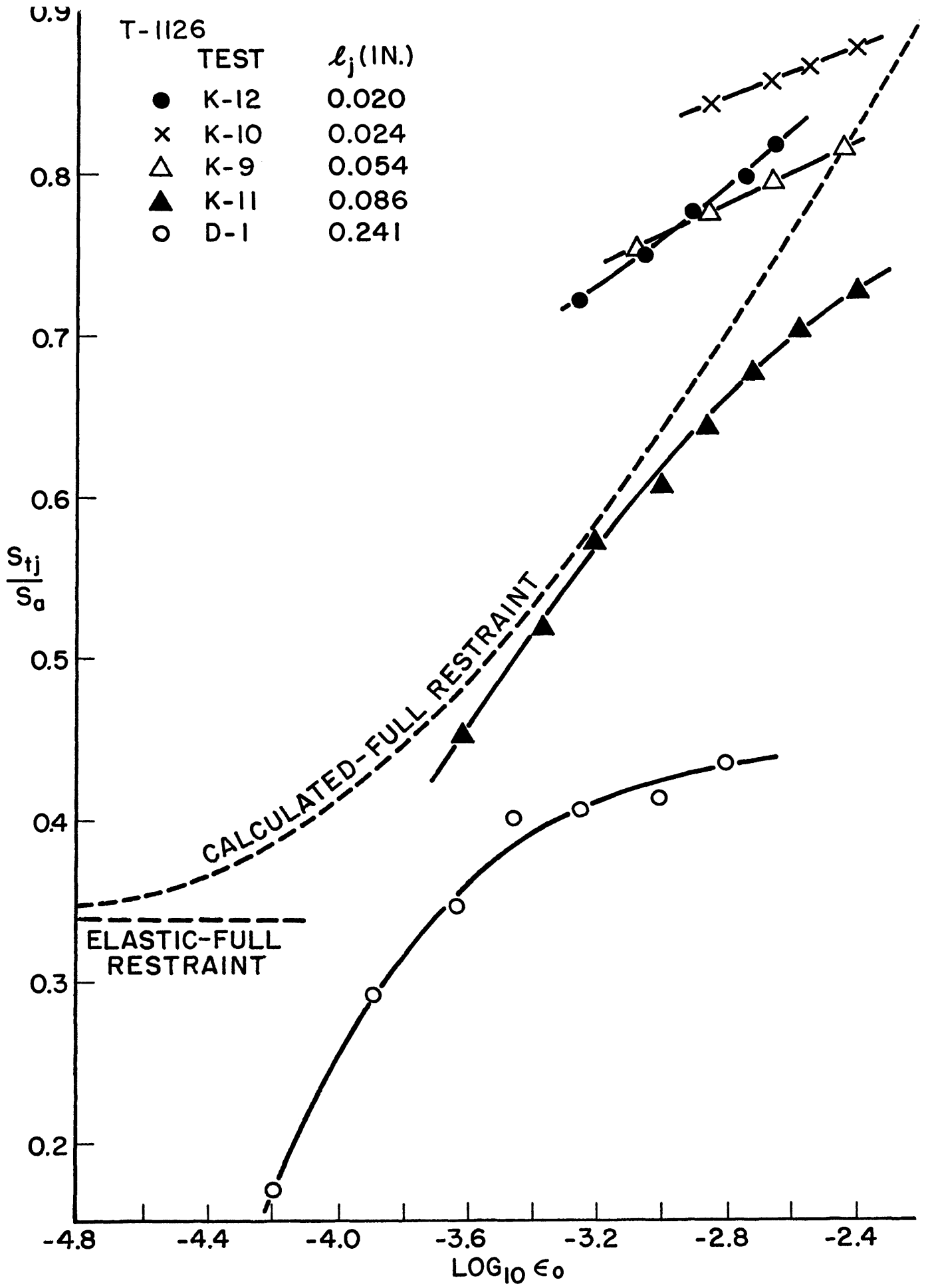

FIGURE 21. PLASTIC TRIAXIALITY AS A FUNCTION OF JOINT LENGTH AND PLASTIC STRAIN

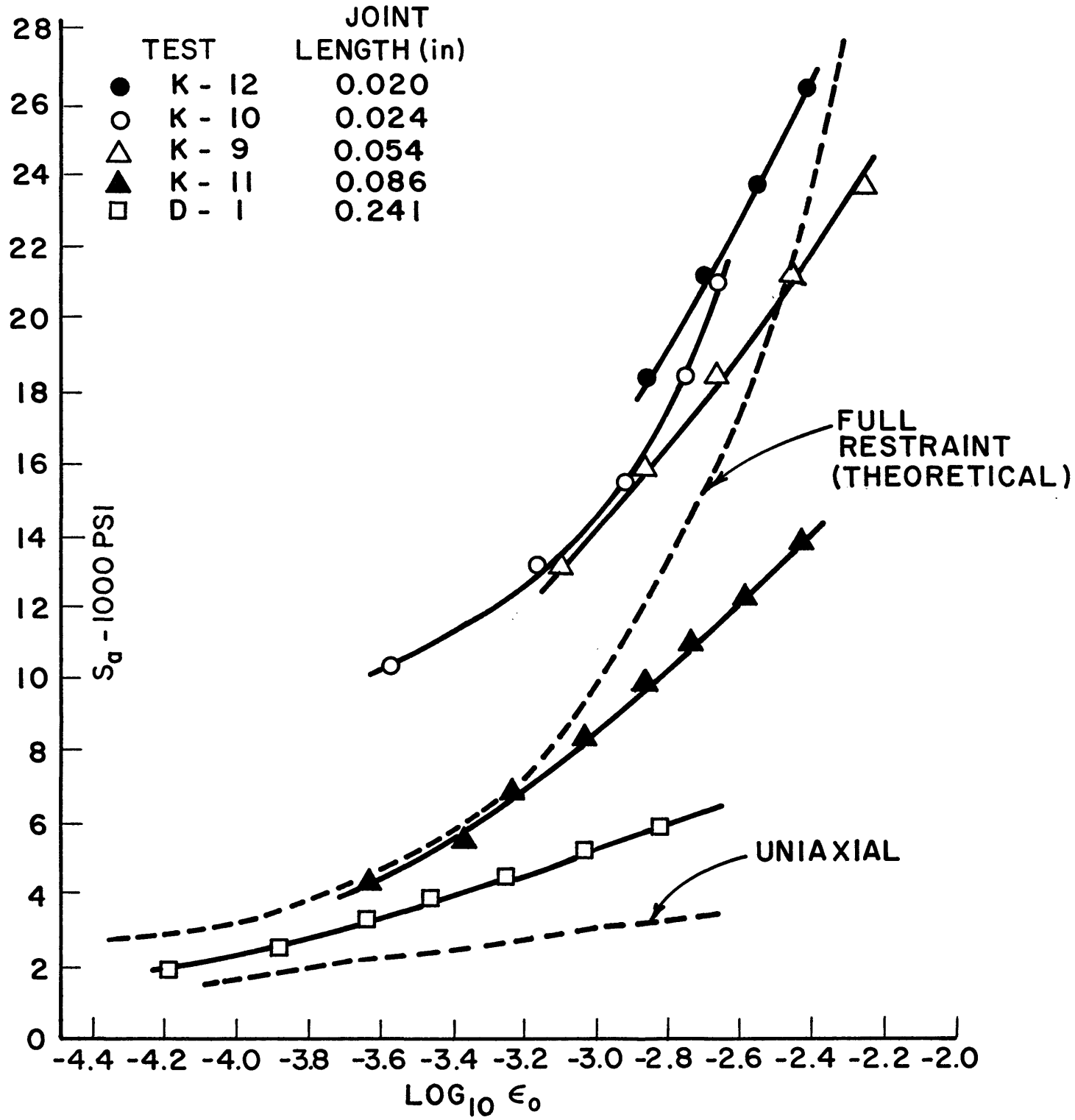

FIGURE 22. RELATIVE TRIAXIALITY VERSUS PLASTIC STRAIN AND JOINT LENGTH. RELATIVE TRIAXIALITY IS EXPRESSED IN TERMS OF AXIAL STRESS

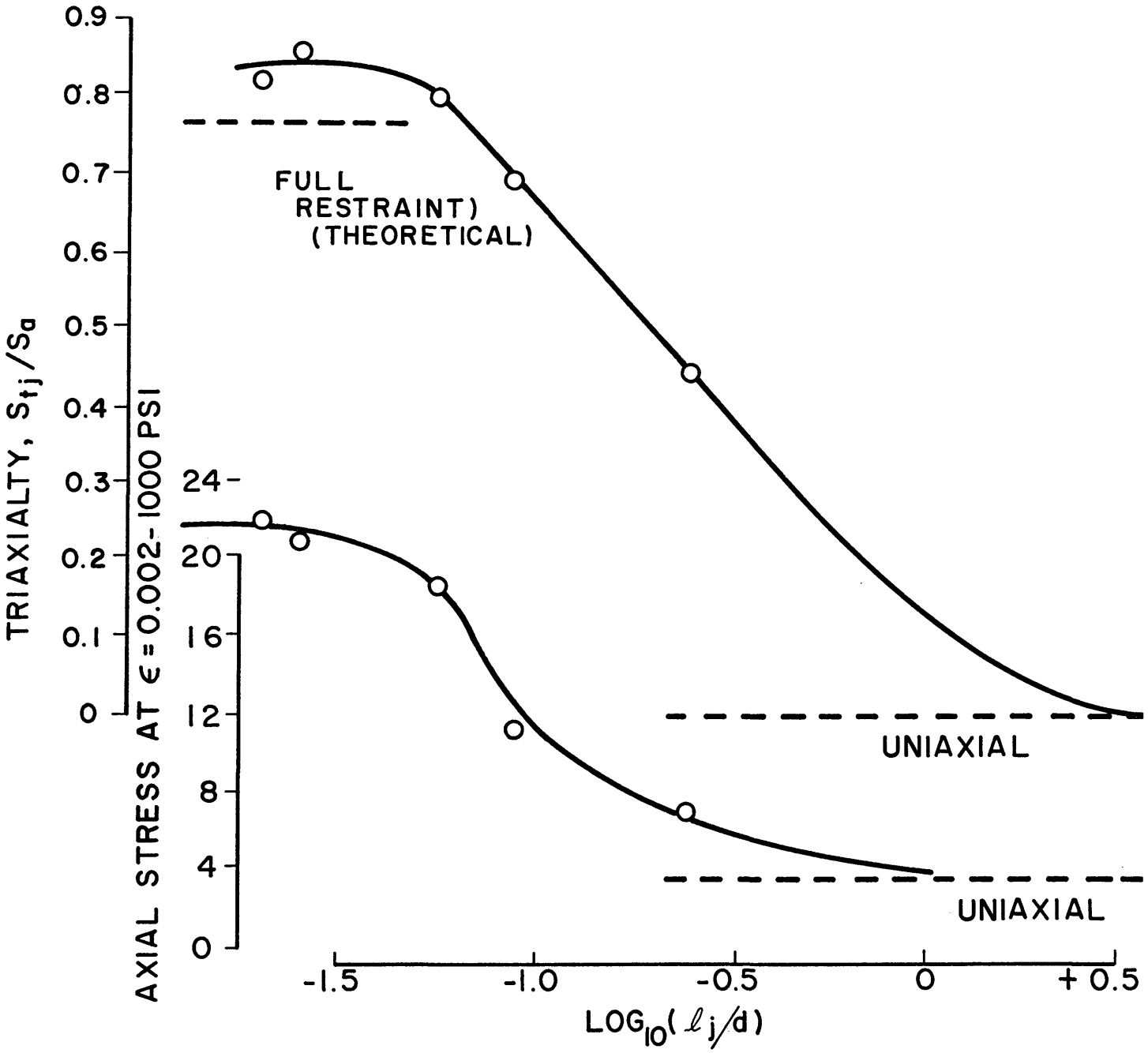

FIGURE 23. TRIAXIALITY AS A FUNCTION OF JOINT LENGTH

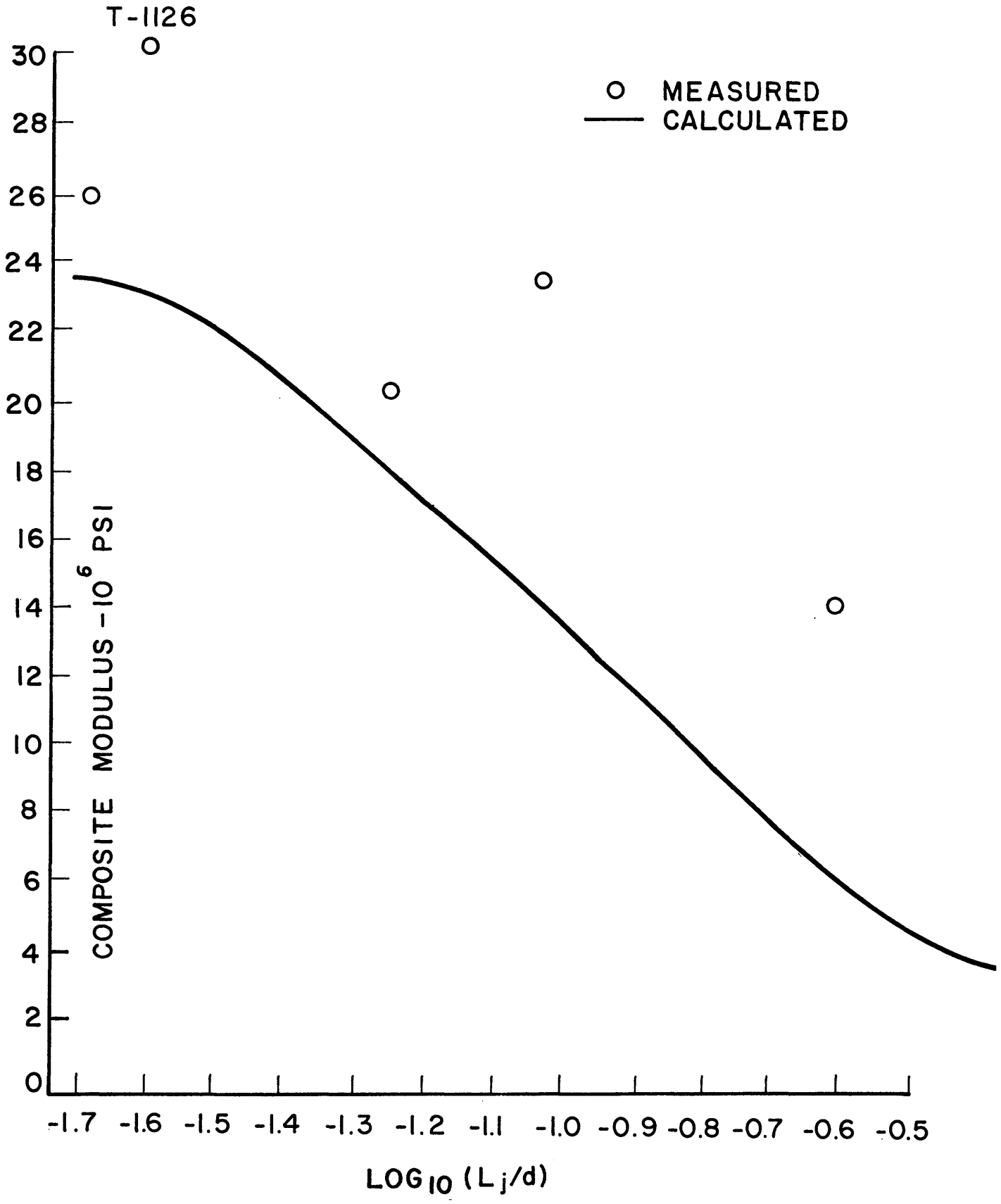

FIGURE 24. EXPERIMENTAL AND THEORETICAL VALUES OF COMPOSITE MODULUS AS A FUNCTION OF RELATIVE JOINT LENGTH

Figure 25. Use of Strobotac for Timing

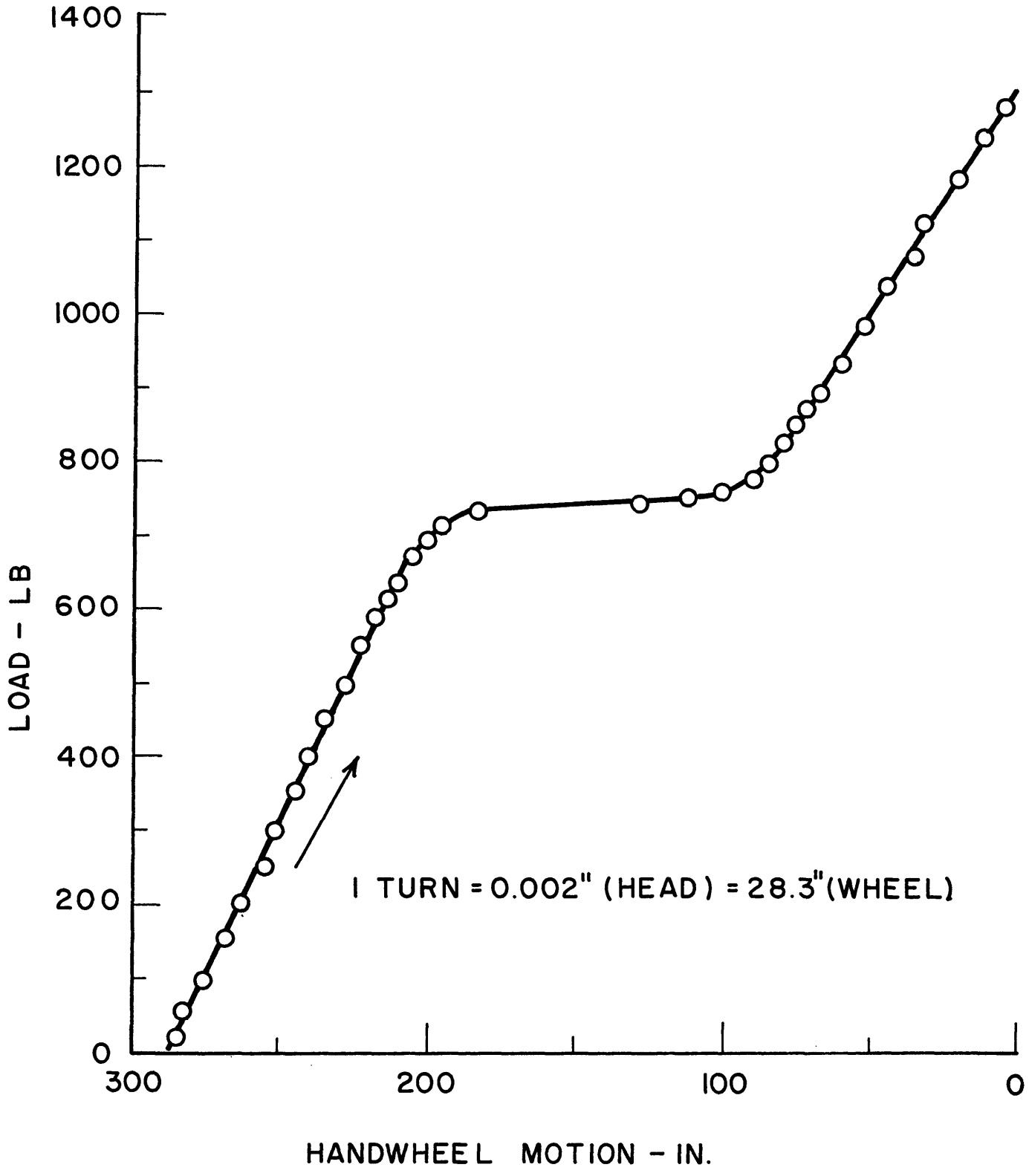

FIGURE 26. TENSILE LOAD VS WHEEL DEFLECTION

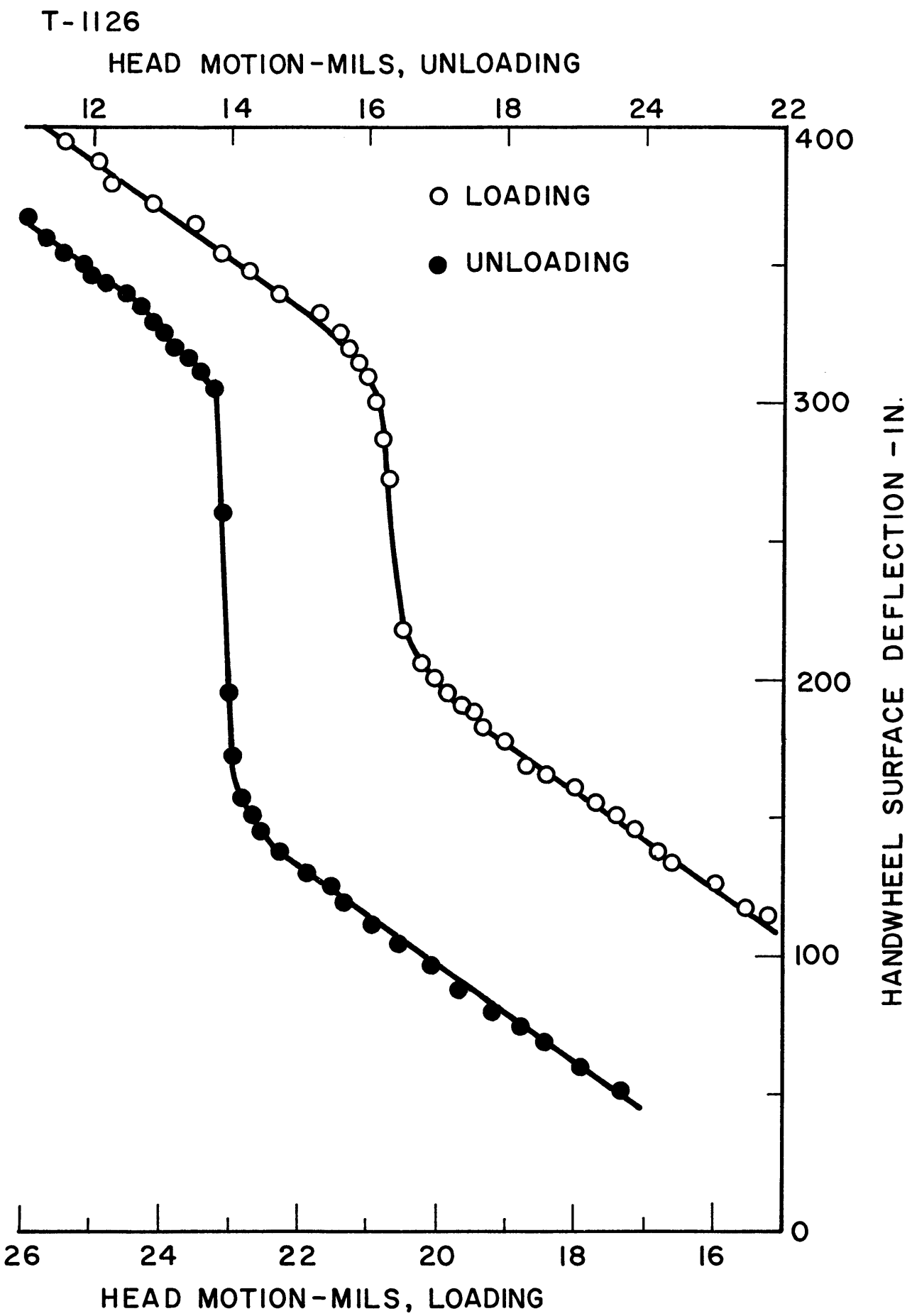

FIGURE 27. HEAD DISPLACEMENT VS WHEEL DEFLECTION

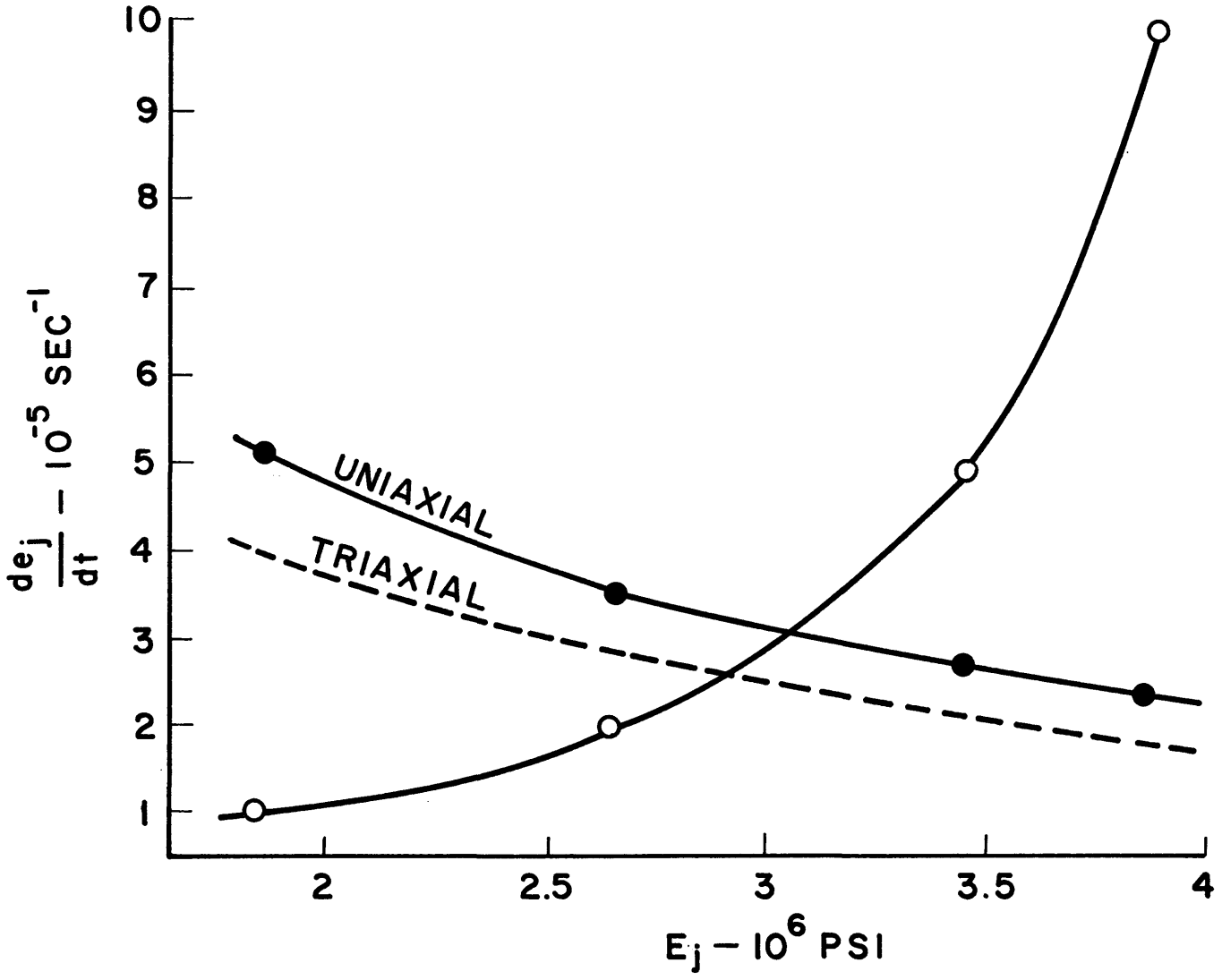

FIGURE 28. DETERMINATION OF MODULUS AN STRAIN RATE FOR TEST K-12 FOR TWO DIFFERENT STRESS STATES